University of Helsinki
Department of Chemistry
Laboratory of Analytical Chemistry
Finland

Asymmetrical flow field-flow fractionation in the study of water-soluble macromolecules

Gebrenegus Yohannes

Academic dissertation

To be presented, with permission of
the Faculty of Science of the University of Helsinki,
for public criticism in Auditorium A110 of
the Department of Chemistry (A.I. Virtasen aukio 1, Helsinki)
on October 26th 2007, at 12 o'clock.

Helsinki 2007

Custos:

Prof. Marja-Liisa Riekkola

Laboratory of Analytical Chemistry

Department of Chemistry

University of Helsinki

Finland

Reviewers:

Dr. Karel Klepárnik

Institute of Analytical Chemistry

Academy of Sciences of the Czech Republic

Czech Republic

And

Prof. Jukka Lukkari

Department of Chemistry

University of Turku

Finland

Opponent:

Prof. Michel Martin

Laboratoire de Physique et Mécanique des Milieux Hétérogènes

UMR CNRS 7636, Ecole Supérieure de Physique et de Chimie Industrielles

10 rue Vauquelin, 75231 Paris Cedex 05

France

ISBN 978-952-92-2628-3 (paperback)

ISBN 978-952-10-4179-2 (PDF file)

http://ethesis.helsinki.fi

Helsinki University Printing House

Helsinki 2007

Table of contents

PREFACE

This thesis is based on research carried out at the Laboratory of Analytical Chemistry of the Department of Chemistry, University of Helsinki, after the Licentiate work in 2002.

I wish to express my deepest gratitude to my supervisor Professor Marja-Liisa Riekkola, Head of the Laboratory of Analytical Chemistry, for offering me the opportunity to carry out this work. I am grateful for her scientific guidance, encouragement, and patience during these extended years, especially during the finalizing of this thesis.

I am greatly indebt to my co-supervisors Docent Susanne Wiedmer and Lic. Phil. Matti Jussila who were always willing to invest their time and energy, helping in my research. Susanne worked hard to introduce the method to other collaborators to utilize it as a research tool. I thank you Susanne, without your support it would have been difficult to come to this stage. Matti solved theoretical, technological, and software problems. I thank you Matti for the kindness and good will you have shown me.

I am grateful to Lic. Phil. Pentti Jyske, Lic. Phil. Sami Varjo, and to Mr Pekka Tarkiainen (in the workshop of the Department of Chemistry) who helped in preparing and assembling the separation channels, fitting tools, and detectors. I am also grateful to Docent Heli Sirén, Professor Kari Hartonen, and Professor Tuulia Hyötyläinen, who shared and contributed their innovative research ideas and helped with many circumstances.

I would like to thank all former and current members of the Laboratory of Analytical Chemistry with all the newcomers who in many different ways have supported and encouraged me through all these years. Many thanks to Professor Tapio Kotiaho, Dr. Juhani Kronholm, Dr. Simo Porras, Dr. Jie Chen, Dr. Jaroslav Pol, Dr. Sami Palonen, Lic. Phil. Pertti Vastamäki, Lic. Phil. Maarit Kivilompolo, Lic. Phil. Maria Lindén, MSc. Jari Hautala, MSc. Kati-Henna Pystynen, MSc. Minna Kallio, MSc. Jaana Muhonen, MSc. Lucia D'Ulivo, MSc. Kati Vainikka, MSc. Jaana Jäntti, MSc. Laura Luosujärvi, MSc. Arvind Verma, MSc. Miika Kuivikko, MSc. Jevgeni Parchintsev, MSc. Totti Laitinen, and MSc. Joonas Nurmi. Special thanks go to MSc. Merit Hortling, Liisa Heino, and Erja Pyykkö who took care that everything was functioning in the laboratory.

I wish to express my sincere thanks to Professor Heikki Tenhu and his group at the Laboratory of Polymer Chemistry, University of Helsinki, for kindly allowing me to use their instrumental methods, and acted as co-authors. In addition I express my thanks to all research collaborators who had shown their interest in the FFF method: Many thanks to Prof. Jukka Lukkari, University of Turku; Prof. Petri Kovanen, docent Katariina Öörni and PhD student Mia Sneck, from Wihuri Research Institute; Docent Matti Jauhiainen, PhD student Niko Setälä, researcher Jari Metso, and Professor Christian Ehnholm from the Department of Molecular Medicine, National Public Health Institute, Biomedicum, Helsinki; Docent Juha Holopainen from the Department of Ophthalmology, University of Helsinki; and Professor Paavo K. J. Kinnunen from Helsinki Biophysics & Biomembrane Group, Institute of Biomedicine, Biomedicum, University of Helsinki.

I am deeply grateful for the pre-examiners, Dr. Karel Klepárnik and Prof. Jukka Lukkari, for their devoted work on the pre-examination of my work and for the constructive comments. Many thanks to Dr. Kathleen Ahonen and Dr. Mary Metzler who revised the language of the publications and the thesis.

My special thanks go to Dr. Nanyin Han, who tried his best to teach me to practice Chinese Taiji.

Finally, my heartfelt and most genuine thanks go to all my family members and friends for their endless love and affection, encouragement and belief in me. Especially my dearest wife Ferewine, my sons Neftalem, Yontale (Yonatan), Saimon and our new born daughter Emilia to whom I dedicate this work, many thanks for standing by me through happy and rough times. You have given me tremendous support, love and understanding throughout the years.

Financial support from the Academy of Finland, Suomen Tiedeseura, Magnus Ehrnrooth foundation, Jenny and Antti Wihuri Foundation, Kemira, and Helsinki University is gratefully acknowledged.

To my family

ABSTRACT

Asymmetrical flow field-flow fractionation (AsFlFFF) was constructed, and its applicability to industrial, biochemical, and pharmaceutical applications was studied. The effect of several parameters, such as pH, ionic strength, temperature and the reactants mixing ratios on the particle sizes, molar masses, and the formation of aggregates of macromolecules was determined by AsFlFFF. In the case of industrial application AsFlFFF proved to be a valuable tool in the characterization of the hydrodynamic particle sizes, molar masses and phase transition behavior of various poly(N-isopropylacrylamide) (PNIPAM) polymers as a function of viscosity and phase transition temperatures. The effect of sodium chloride salt and the molar ratio of cationic and anionic polyelectrolytes on the hydrodynamic particle sizes of poly (methacryloxyethyl trimethylammonium chloride) and poly (ethylene oxide)-block-poly (sodium methacrylate) and their complexes were studied. The particle sizes of PNIPAM polymers, and polyelectrolyte complexes measured by AsFlFFF were in agreement with those obtained by dynamic light scattering. The molar masses of PNIPAM polymers obtained by AsFlFFF and size exclusion chromatography agreed also well. In addition, AsFlFFF proved to be a practical technique in thermo responsive behavior studies of polymers at temperatures up to about 50 ^{o}C.

The suitability of AsFlFFF for biological, biomedical, and pharmaceutical applications was proved, upon studying the lipid-protein/peptide interactions, and the stability of liposomes at different temperatures. AsFlFFF was applied to the studies on the hydrophobic and electrostatic interactions between cytochrome c (a basic peripheral protein) and anionic lipid, and oleic acid, and sodium dodecyl sulphate surfactant. A miniaturized AsFlFFF constructed in this study was exploited in the elucidation of the effect of copper (II), pH, ionic strength, and vortexing on the particle sizes of low-density lipoproteins.

LIST OF ORIGINAL PUBLICATIONS

The dissertation is based in the following five publications, thereafter referred to by their Roman numerals (I-V):

I. **Cytochrome c-dimyristoylphosphatidylglycerol interactions studied by asymmetrical flow field-flow fractionation.** Gebrenegus Yohannes, Susanne K. Wiedmer, Esa K. J. Tuominen, Paavo K. J. Kinnunen, and Marja-Liisa Riekkola, *Anal. Bioanal. Chem.,* 380 (2004) 757-766. Copyright 2004 Springer Science and Business Media.

II. **Characterization of poly (N-isopropylacrylamide) by asymmetrical flow field-flow fractionation, dynamic light scattering, and size exclusion chromatography.** Gebrenegus Yohannes, Jun Shan, Matti Jussila, Markus Nuopponen, Heikki Tenhu, and Marja-Liisa Riekkola, *J. Sep. Sci.,* 28 (2005) 435-442. Copyright 2005 Wiley-VCH Verlag GmbH & Co. KGaA.

III. **Polyelectrolyte complexes of poly (methacryloxyethyltrimethylammonium chloride) and poly(ethylene oxide)-block-poly(sodium methacrylate) studied by asymmetrical flow field-flow fractionation and dynamic light scattering.** Gebrenegus Yohannes, Susanna Holappa, Susanne K.Wiedmer, Toni Andersson, Heikki Tenhu, and Marja-Liisa Riekkola, *Anal. Chim. Acta*, 542 (2005) 222-229. Copyright 2005 Elsevier Science.

IV. **Stability of phospholipid vesicles studied by asymmetrical flow field-flow fractionation and capillary electrophoresis.** Gebrenegus Yohannes, Kati-Henna Pystynen, Marja-Liisa Riekkola, and Susanne K.Wiedmer, *Anal. Chim. Acta,* 560 (2006) 50-56. Copyright 2006 Elsevier Science.

V. **Miniaturization of asymmetrical flow field-flow fractionation and application to studies on lipoprotein aggregation and fusion.** Gebrenegus Yohannes, Mia Sneck, Sami J.O. Varjo, Matti Jussila, Susanne K. Wiedmer, Petri T. Kovanen, Katariina Öörni, and Marja-Liisa Riekkola, *Anal. Biochem.*, 354 (2006) 255-265. Copyright 2006 Elsevier Science.

PAPERS NOT INCLUDED IN THIS THESIS

1. **Flow field-flow fractionation in the study of dairy products.** Matti Jussila, Gebrenegus Yohannes and Marja-Liisa Riekkola, *J. Microcolumn Sep.*, 9 (1997) 601-609.

2. **Ultrathin polyelectrolyte multilayers in situ ESR/UV-Vis-NIR spectroelectrochemical study of charge carriers formed under oxidation.** Peter Rapta, Jukka Lukkari, Ján Tarábek, Mikko Salomäki, Matti Jussila, Gebrenegus Yohannes, Marja-Liisa Riekkola, Jouko Kankare and Lothar Dunsch, *Phys. Chem. Chem. Phys., 6 (2004) 434-441*.

3. **Fractionation of humic substances by asymmetrical flow field-flow fractionation.** Gebrenegus Yohannes, Susanne K. Wiedmer, Matti Jussila, and Marja-Liisa Riekkola, *Chromatographia*, 61 (2005) 359-364.

4. **Open tubular capillary electrochromatography: technique for oxidation and interaction studies on human low-density lipoproteins.** Ruth Kuldvee, Lucia D'Ulivo, Gebrenegus Yohannes, Petrus W. Lindenburg, Minna Laine, Katariina Öörni, Petri Kovanen, and Marja-Liisa Riekkola, *Anal. Chem.*, 78 (2006) 2665-2671.

5. **Interfacial and lipid lransfer lroperties of human phospholipids transfer protein: implications for the t**ransfer m**echanism of p**hospholipids.** Niko L. Setälä, Juha M. Holopainen, Jari Metso, Susanne K. Wiedmer, Gebrenegus Yohannes, Paavo K. J. Kinnunen, Christian Ehnholm, and Matti Jauhiainen, *Biochemistry*, 461 (2007) 1312-1319.

6. **Comprehensive two-dimensional field-flow fractionation–liquid chromatography in the analysis of large molecules.** Gebrenegus Yohannes, Susanne K. Wiedmer, Jaakko Hiidenhovi, Ari Hietanen, and Tuulia Hyötyläinen, *Anal. Chem.*, 79 (2007) 3091-3098.

7. **Open tubular capillary electrochromatography: A new technique for in situ enzymatic modification of low density lipoprotein particles and their protein-free derivatives.** Lucia D'Ulivo, Gebrenegus Yohannes, Katariina Öörni, Petri. T. Kovanen and Marja-Liisa Riekkola. *The Analyst (in press*), published on the web: 30 July 2007, (DOI: 10.1039/b706249d).

ABBREVIATIONS

(μ-TAS)	micro scale total analysis systems
α-CT	α-chymotrypsin
σ_d	standard deviation
AAAS	American association for the advancement of science
AFM	atomic force microscope
AsFlFFF	asymmetrical flow field-flow fractionation
AUC	analytical ultracentrifugation
BSA	bovine serum albumin
C	concentration relative to an accumulation wall
C_0	concentration at an accumulation wall
CE	capillary electrophoresis
CHF	capillary hydrodynamic fractionation
cyt c	cytochrome c
d_H	hydrodynamic diameter (nm)
DLS	dynamic light scattering
d_{mean}	average (mean) diameter (nm)
DMPG	1,2-dimyristoyl-*sn*-glycero-3-[phospho-*rac*-(1-glycerol)](sodium salt)
ElFFF	electrical field-flow fractionation
EOF	electroosmotic flow
EPC	egg yolk phosphatidylcholine
F	force on the analyte due to the applied field
f	frictional coefficient
FFF	field-flow fractionation
FlFFF	flow field-flow fractionation

H	plate height
HDC	hydrodynamic chromatography
HDL	high-density lipoproteins
HF FlFFF	hollow fiber flow FFF
IDL	intermediate density lipoprotein
IS	ionic strength
LCST	lower critical solution temperature
LDL	low-density lipoprotein
LOD	limit of detection
LUV	large unilamellar vesicles
mAsFlFFF	miniaturized asymmetrical flow field-flow fractionation
MG	molten globule
MLV	multilamellar vesicles
OA	oleic acid
PA	phosphatidic acid
PC	phosphatidylcholine
PDI	polydispersity index
PE	polyelectrolyte
PEC	polyelectrolyte complex
PEO	polyethylene oxide
PEO-b-PMAA	poly (ethylene oxide)-block-poly (sodium methacrylate)
PG	α-phosphatidyl-*dl*-glycerol
PLA2	phospholipases A2
PMOTAC	poly-(methacryloxyethyl trimethylammonium chloride)
PNIPAM	poly-N-isopropylacrylamide
POPC	1-palmitoyl-2-oleyl-*sn*-glycero-3-phosphatidylcholine

PS	phosphatidylserine
PSS	polystyrene sulphonate standards
R	retention ratio
RAFT	reversible addition-fragmentation chain transfer
R_s	resolution
SdFFF	sedimentation FFF
SDS	sodium dodecyl sulphate
SDS-PAGE	sodium dodecyl sulfate polyacrylamide gel electrophoresis
SEC	size exclusion chromatography
SEM	scanning electron microscope
SMase	sphingomyelinase
SUV	unilamellar vesicle
TEM	transmission electron microscope
ThFFF	thermal FFF
VLDL	very low-density lipoprotein

SYMBOLS

$\langle U \rangle$	external field (cm s^{-1})
$\langle V \rangle$	average velocity of analyte zone (cm s^{-1})
ω	angular velocity (rad s^{-1})
$\dot{V}$	channel flow rate, volumetric (ml min^{-1})
$\dot{V}_c$	cross flow rate, volumetric (ml min^{-1})
z'	focusing position
χ	dimensionless non-equilibrium zone broadening parameter
ρ	carrier density (g mol^{-1})
λ	retention parameter
η	viscosity of carrier liquid ((Pa*s), (1 mPa*s = 1 centipoise (*cp*))
σ_d	standard deviation
D	diffusion coefficient (cm^2 s^{-1})
k	Boltzmann constant (1.38×10^{-23} JK^{-1})
l	layer thickness (cm)
M	molar mass (g mol^{-1})
N_A	Avogadro's number (6.022×10^{23} mol^{-1})
r_H	hydrodynamic radius (nm)
R_g	gas constant (8.314472 J mol^{-1} K^{-1})
T	absolute temperature (273 K)
t^0	void time (s, min)
t_r	retention time (s, min)
V^0	void volume or geometric channel volume (ml)
w	channel thickness (μm, cm)

1. GENERAL PARTICLE SIZE ANALYSIS

A. Introduction

In industry, information on particle sizes and size distributions is needed for the control and optimization of manufacturing processes, and for the evaluation of product quality. In environmental science, the formation of aerosol particles, and the particles formed in soil and water play an important role. Particle size is significant in many areas of life sciences, from the determination of sizes of biological particulate materials to understanding the causes of diseases and finding their cures. In addition, the sizes and characteristics of particles affect the physical stability, chemical reactivity, solubility, and strength of many materials. The techniques employed for particle size measurements are based on various principles: some utilize light scattering, others measure the motion of the particles in response to some force, such as gravity, centrifugal force, viscous drag, Brownian motion, or electrostatic force. Microscopy, light scattering, centrifugation, chromatography, electrophoresis, and field-flow fractionation are some of the most widely used techniques for the determination of particle sizes.

1.1. Microscopy

Transmission Electron Microscopy: The easiest way to measure particle size is to look at the particles using optical (light) microscopy. A light microscope is simple, but if the average particle size is below 1 μm, it is not recommended. Sub-micrometric particle sizes are generally most relevant for industrial and biological applications, for which other microscopic methods, such as electron microscopy and atomic force microscopy are frequently employed. The transmission electron microscope (TEM) was the first type of electron microscope to be developed and is constructed exactly like the light microscope except that a focused beam of electrons is used instead of light to "see through" the specimen. Max Knoll and Ernst Ruska in Germany built the first TEM instrument in 1931 [1]. The technique quickly surpassed the resolution of light microscopy, and in 1938 the first commercial instrument was produced by Siemens-Halske Company in Berlin, in which magnetic lenses focused the electron beam,

replacing glass lenses. Later, in 1970, high-resolution transmission electron microscopy emerged [2]. With electron transmission microscopes, macromolecular structure at a single-particle level can be seen [3]. The magnification power for TEM reaches up to 300000x, whereas for light microscopes it is only from 1000x to 2000x.

Scanning Electron Microscope: The principle of the scanning electron microscope (SEM) emerged in 1935 by Knoll (1935). Subsequently von Ardenne constructed a scanning electron microscope (SEM) by adding scan coils to a transmission electron microscope [4]. The first commercial instruments appeared just around 1965 due to the late development of suitable electronics for "scanning" the beam of electrons across the sample [5]. Scanning electron microscopy examines structure by bombarding the specimen with a scanning beam of electrons, and then the slow-moving secondary electrons that the specimen generates are collected, amplified, and displayed on a cathode ray tube. The electron beam and the cathode ray tube scan synchronously so that an image of the surface of the specimen is formed. Specimen preparation includes drying the sample and making it conductive to electricity, if it is not already. SEM is typically used to examine the external structure of objects that are as varied as biological specimens, rocks, metals, ceramics and almost anything that can be observed in a dissecting light microscope. At the same time, information on particle size can usually be obtained. Cryo-electron microscopy partially overcomes the difficulties related to low tolerance towards bombardment of electrons by quick-freezing the sample at -150 ^{o}C in e.g., liquid ethane.

1.2. Scanning probe/atomic force microscopy

Scanning probe microscopy (SPM) defines for a group of instruments used to image and measure properties of material, chemical, and biological surfaces. SPM images are obtained by scanning a sharp probe across a surface while monitoring and compiling the tip–sample interactions to provide an image. The two primary forms of SPM are scanning microscopy (STM) and atomic force microscopy (AFM). STM wad developed in 1982, that can image conducting or semiconducting surfaces [6] AFM was developed later in 1986, and has become a versatile tool for both nanoscale-imaging of surfaces and for the measurement of many intermolecular and surface forces [7-10]. In AFM, forces between a probe and the

relevant surface are measured through changes in the deflection of a flexible cantilever attached to the probe. For image collection, it is assumed that changes in sample topography affect the probe-sample interaction profile and therefore affect the response of the cantilever.

In AFM, there are several modes of operation, e.g., the contact mode and the tapping mode. The contact mode AFM measures topography. When the cantilever tip makes contact with the sample surface, according to the Hookian spring force relationship its deflection is proportional to the force acting on the probe. Either the repulsive force between the tip and the sample or the actual tip deflection is recorded relative to spatial variation and then is converted into an analogue image of the surface. Cantilever displacements are then amplified by corresponding deflections of a laser beam reflected into a split photodiode from the upper surface of the probe.

Although operation in contact mode has proven successful, it suffers from drawbacks that limit its use on a number of sample types. The constant downward force on the tip often damages (and thus changes) the sample, especially those with softer surfaces such as polymers and biological samples. This drawback in contact mode has been addressed through the development of tapping mode AFM [11]. In tapping mode the probe tip is not in continuous contact with the surface (referred to as contact mode), but oscillates rapidly up and down as it is scanned over the surface, essentially tapping its way gently, but firmly and rapidly, and sensing the height of features it encounters. Tapping mode AFM eliminates the shear force present in contact mode. Tapping mode is therefore the method of choice for most applications, particularly those involving polymers. Generally AFM offers the capability to visualize in 3D, and can give both qualitative and quantitative information on many physical properties including size, morphology, surface texture and roughness. Statistical information on size, surface area, and volume distributions can be determined as well. A wide range of particle sizes can be characterized in the same scan, from about 1 nanometer (nm) to about 8 micrometers (μm). In addition, AFM can characterize nanoparticles in multiple media such as ambient air and liquid [12, 13, 14, 15].

1.3. Flow cytometry

Flow cytometry is a technology that simultaneously measures and then analyzes multiple physical characteristics of a single particle, usually from cells, as the cells flow in a fluid stream through a beam of light. The technique also analyzes the granularity or internal complexity of cellular objects. The technique is made up of three main features: fluidics, optics, and electronics. The fluidics system transports particles to the laser beam for interrogation. The optics system consists of lasers to illuminate the particles in the sample stream and optical filters to direct the resulting light signals to the appropriate detectors. The electronics system converts the detected light signals into electronic signals that can be processed by the computer. Any suspended particle or cell from 0.2–150 μm in size is suitable for analysis. Cells from solid tissue must be disaggregated before analysis. For some instruments equipped with a sorting feature, the system is capable counting number of particles [16 -18].

1.4. Dynamic light scattering

The determination of particle sizes by direct microscopic observations is convincing, though it may have some drawbacks, such as that samples need to be dried during preparation, and that because the amount needed is tiny, it may not represent the whole sample. For this reason, other alternative and non-destructive methods, such as dynamic light scattering (DLS), have been developed. In 1960s, the dynamic light scattering method was described for the first time by Mueller and Givens [19]. Later, during the 1970s, the digital correlation function was introduced to reduce the analysis time from many hours to a few seconds [20]. Since then DLS has become a widely recognized method for determining average particle size of e.g. water-soluble polymers, organic soluble polymers and colloids. The detailed theory behind this method was developed by Berne and Peccora 1975 [21], Brown 1993 [22], and Finsy 1994 [23]. DLS measures the variation in scattered light intensity due to random Brownian motion as a function of time at a given scattering angle. Analysis of these intensity fluctuations enables the determination of the distribution of diffusion coefficients of the particles, which are converted into a size distribution using established theories. For spheres,

the Stokes-Einstein relationship relates the diffusion coefficient (*D)* to the hydrodynamic diameter (d_H*)* by:

$$D = \frac{kT}{3\pi\eta d_H} \quad (1)$$

where *T* is the absolute temperature, *k* is the Boltzmann constant, and η is the viscosity of the suspending liquid. The particle size can, therefore, be measured by DLS using Equation 1. During the DLS measurement, an autocorrelation function is generated from the fluctuation of scattered light intensity, and this function, a decaying exponential function, is inverted to obtain the diffusion coefficient or the particle size by applying the above Stokes-Einstein equation. For the determination of particle size distribution, analysis of the autocorrelation function is done by numerically fitting the data using Equation 1, with assumed Gaussian distributions for spherical or nearly spherical shapes.

By varying the scattering angle, dynamic light scattering measurements can cover an extended range of particle sizes, starting from about 3 nm to about 7 μm [24]. The upper size limit of the technique is more or less density dependent, as dynamic light scattering requires the particles to be randomly diffusing. This places the upper size limit at the point where sedimentation of the particles dominates the diffusion process. The lower size is dependent on the excess scattered light that the sample generates compared to the suspending medium. Many factors will contribute to this lower size limit including the sample concentration, the relative refractive index (i.e. the particle refractive index compared to the medium refractive index), laser power and wavelength, sensitivity of the detector and optical configuration of the instrument.

1.5. Analytical ultracentrifugation

In 1924, Svedberg and Rinde developed an instrumental technique for particle size analysis that was based on sedimentation [25]. The system was later patented by Oliver, Hicken and Orr, and commercialized in 1969 by Micrometrics into an instrument known as the Sedigraph. [26]. In a sedimentation velocity experiment, application of a sufficiently large centrifugal force field leads to movement of solute molecules toward the bottom of the centrifuge cell.

The rate of sedimentation in a centrifugal field is described by the Svedberg equation as:

$$s = \frac{v}{\omega^2 r} = \frac{M(1-\bar{v}\rho)}{N_A f} = \frac{MD(1-\bar{v}\rho)}{R_g T} \qquad (2)$$

where s is the sedimentation coefficient, v is the velocity of the molecule, ω is the angular velocity of the rotor, r is the radial distance from the center of rotation, $\omega^2 r$ is the centrifugal field strength, M is the molar mass, f is the frictional coefficient (which is directly related to macromolecular shape and size), ρ is the density of the solvent, N_A is Avogadro's number, $\bar{v}$ is the partial specific volume of the solute, D is the diffusion coefficient, and R_g is the gas constant. The solvent parameters (density and viscosity) are experimentally measurable, or can be calculated from the solvent composition using tabulated data.

In an analytical ultracentrifuge, a sample being spun can be monitored through an optical detection system, typically a UV/VIS detector. This allows the operator to observe changes in sample concentration versus the axis of rotation in the centrifugal field. With modern instrumentation, observations are electronically digitized and information related to hydrodynamic particle size is retrieved [27, 28]. Most analytical centrifugation methods are designed principally for the analysis of very fine particulates. The upper size range tends to be rather low (typically between 2 µm and 10 µm). At the lower size end, the analysis range can be extended down to about the size of proteins, depending on the speed of the centrifuge and the sensitivity of the detection system [29].

1.6. Size exclusion/Hydrodynamic chromatography

Size exclusion chromatography (SEC) is a proven analytical method used for the separation of macromolecules according to their molecular size. In this technique, the molecules in solution flow through the porous packed bed of a column. The size range (2–10 µm) of the pores in the beads determines whether particles are totally excluded, partially excluded or have full entry into all beads. Particles that are totally excluded have the shortest residence time on the column, whereas particles that have full entry into the beads have the longest residence time. Partially excluded particles have residence times between the two. On this basis, particles of different sizes are separated.

Separation of macromolecules according to size is most often done by size exclusion chromatography, and in some special cases by hydrodynamic chromatography (HDC) which uses non porous packing materials [30 - 33], or by capillary hydrodynamic fractionation (CHF) which uses a long open tubular capillary for the separation of particles according to size. In HDC, the speed of flow, *v*, due to a pressure difference, is given as a function of the distance from the channel wall, *r*, by:

$$v(r) = v_{\max} = (1 - \frac{r^2}{a^2}) \qquad (3)$$

where *a* is the channel radius.

Due to the parabolic profile given by this function particles have different velocities depending on their position in the column, and a plug of material travelling in the column will spread out. This has impact on the resolution of a separation, but it can also be used to separate particles by size. It is the position of the hydrodynamic center of mass that determines particle velocity, and since larger particles are excluded from the area near the wall, they reallocate in the faster central flow.

Hydrodynamic chromatography is not a variant of SEC, although the process of packing the column material and the order of fractionation of particles from large to small are similar in both methods. The advantage of CHF over SEC is the absence of a porous stationary phase, which eliminates the slow formation of equilibrium due to the slow diffusion of macromolecules, thereby reducing the dispersion dramatically.

1.7. Gel electrophoresis

Gel electrophoresis is commonly used in many clinical laboratories to separate macromolecules according to their mobility in a gel in response to an electric field. Acrylamide, cross-linked with N,N'-methylene bisacrylamide is usually used as a gel. A small drop of sample is deposited at one end of the porous gel, which is in contact at both ends with reservoirs containing solution. When an electric field is applied at the ends of the gel,

molecules dissolved in the conducting solution move through the gel. Once the electric current is stopped, the position of the band allows the determination of the size and charge of the particles. Thus, with a uniform gel, the distance of migration is a function of the size of the particle, its charge, and the duration of the electrophoresis [34]. After the separation is complete, the resulting bands are detected, usually by means of a staining reagent that causes them to become visible. The most widely utilized method in proteomics studies is 2D-gel electrophoresis, which was developed by O'Farrell, in 1975 [35]. This method separates proteins according to their isoelectric points in the first dimension in a process called isoelectric focusing, and according to size in the second dimension using sodium dodecyl sulfate polyacrylamide gel electrophoresis (SDS-PAGE) [36 - 38]. 2D-gel electrophoresis is a popular method among biologists even though it suffers from many limitations, such as low sensitivity and lack of precision. [39].

As slab-gel electrophoresis is labor-intensive and produces poorly defined spots, which may be difficult for quantitative analysis, considerable efforts are currently focused on developing capillary electrophoresis (CE). Thus, CE, with polymer solutions acting as a sieving matrix, has become an attractive separation technique for the separation of DNA fragments due to its high efficiency and fast speed of analysis as compared to the conventional slab-gel electrophoresis [40 - 42].

1.8. Field-flow fractionation

Field-flow fractionation (FFF) is among the most important analytical methodologies for the separation and characterization of macromolecules and particles. In terms of biological applications, it can be used to separate particles that range in size from a protein to an entire cell. DNA, viruses, and other macromolecules and complexes, such as lipoproteins, ribosomes, and liposomes, have all been separated using these techniques [43 - 48].

In industry, FFF is used in quality control applications, and in the separation of various colloids and particles such as silica, metal and ceramic particles, as well as in the separation and characterization of various synthetic polymers. FFF has also been used to separate various environmentally relevant particles present in water and soil. Overall, FFF is a very effective

method for both separation and characterization of many different macromolecules. FFF is the method of choice in the present doctoral thesis, and its principle is described in detail in chapter 2.

B. Comparison of techniques employed in particle size measurements

Particle size measurement techniques commonly used in characterizing macromolecules, colloids and submicrometer particles are listed in Table 1. Size ranges are approximate, and actual size ranges vary significantly, depending not only on the instrumental technique, but also on the test material. In many separation techniques, including HDC, SEC, FFF, and AUC (analytical ultracentrifugation), the methods offer particle size distribution, and analytes can be collected for further analysis, except for AUC. Non-fractionation techniques, such as DLS, are fast and reliable for determination of average particle size. However, they are less suited to the analysis of samples with multimodal particle size distributions (e.g. containing monomers and aggregates); the results are often skewed in favor of the size of the aggregates. Among the fractionation techniques used, some only work well in connection with appropriate, selective and sensitive detectors. Particle composition may also influence the limit of detection (LOD). Electron microscopy techniques such as TEM and SEM certainly are powerful techniques for topographical and internal structural analysis, and even results at the single particle level can be achieved. But unfortunately, SEM is sample destructive, in contrast to AFM.

Table 1. *Techniques for particle size analysis.*

Method	Applicable range	Features and benefits	Limitations
Light Microscopy	>1µm	Single particle technique	Low resolution (0.2µm)
TEM	>1nm	Single particle technique	Sample preparation very complex
			Must be performed in vacuum
			Costly
SEM	>10 nm	Single particle technique	Sample preparation very complex
		2D image	Must be performed in vacuum
			Destructive and costly
AFM	~1nm - ~8µm	Single particle technique	Costly but much less than SEM/TEM
		3D image of particle obtained	
		Quantitative analysis on particle distribution obtained	
		Can determine type of force	
		Works at ambient temperature	
		Works both in air and liquid	
		Requires less space and is simpler to operate than SEM/TEM	
Flow cytometry	0.2 - 150 µm	Single particle technique	Costly
		Counting number of particles	
DLS	~3nm - ~7µm	Fast and automatic	Low resolution (~3:1 modal separation)
		Average particle size obtained	Sensitive to dust
		No calibration needed, Non-destructive	Inconvenient for polydisperse PSD
SEC	5kDa-1000kDa	Validated separation technique	Less important for aggregated particles
		Estimates Mw and particle size	Calibration needed for Mw or, size
		Apparent MMD and PSD obtained	Sample clogging of column possible
		Non-destructive	High shear forces
HDC	20nm - ~3um	Apparent PSD directly obtained	Calibration needed for molar mass, size
		Non-destructive	High shear forces
AUC	~2nm - 10µm	Free on sample-column interaction	Dependence on density
		Non-destructive	
		Gives size and shape of molecules	
FFF	~2nm - 50µm	No standard required for size	Upper limit 1µm unless run in steric mode
		Average particle size obtained	Calibration needed for molar mass
		Apparent PSD directly obtained	Calibration needed in steric mode
		Low shear forces	
		Non-destructive	

2. FIELD-FLOW FRACTIONATION (FFF)

Giddings introduced field-flow fractionation (FFF) in 1966 as a process applicable to macromolecules and colloidal separations [49]. Subsequently, several FFF variants were developed, of which the major ones are sedimentation FFF, thermal FFF, electrical FFF, and flow FFF. The advantage of these techniques stems from the single-phase nature of FFF. The basic setup for all the FFF techniques is shown in Figure 1. Carrier liquid is pumped in at one end. A sample, added to the carrier using an injection port or another pump, emerges at the other end for detection and collection. The choice of a detector is similar to SEC, depending on the type of sample rather than the technique. A separation channel, approximately 10 to 50 cm long, 1-3 cm wide and 0.01 to 0.05 cm thick, is at the center of the FFF subtechniques. The channel essentially consists of two "walls"; one of which is an upper wall and the other of which is an accumulation wall.

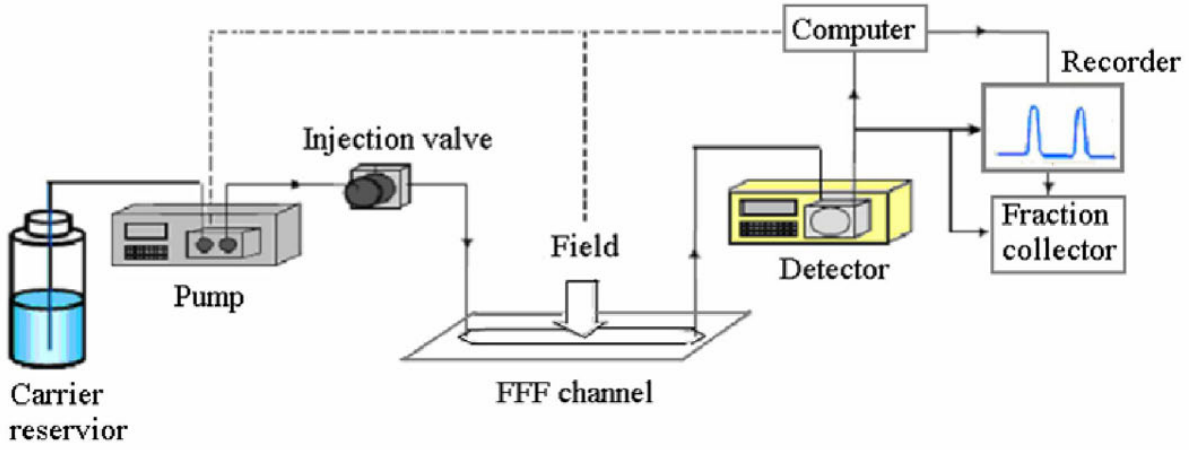

Figure 1. *Basic setup for FFF sub-techniques.*

Inside the channel, the flow obeys a parabolic flow profile (laminar Newtonian flow) similar to the laminar flow in capillary tubes. After injection sample molecules are distributed homogeneously across the channel thickness (w), and are being pushed to the bottom of the channel by the applied external force (centrifugal, thermal, electric or hydrodynamic). Finally, an exponential concentration distribution at the accumulation wall is built up. Since the accumulation wall acts as a barrier to the particles, the net movement of the sample species towards the external field is caused by diffusion from an area of high concentration at the accumulation wall to an area with lower concentration.

The accumulation of the particles at the wall is therefore opposed by diffusion, which carries the particles towards the external field. After a certain relaxation period, a dynamic steady-state is reached. The equation:

$$\frac{C}{C_0} = \exp(-\frac{y}{l}) \tag{4}$$

describes the concentration distribution in the y-direction, which is perpendicular to the accumulation wall (Figure 2). C_0 is the maximum concentration at the wall (y = 0) and C is the concentration at a distance y from the wall; l, a mean layer thickness (thickness of particle layer from the wall). The ratio of the diffusion coefficient (D) to the velocity induced by the external field $\langle U \rangle$ is given by:

$$l = \frac{D}{\langle U \rangle} \tag{5}$$

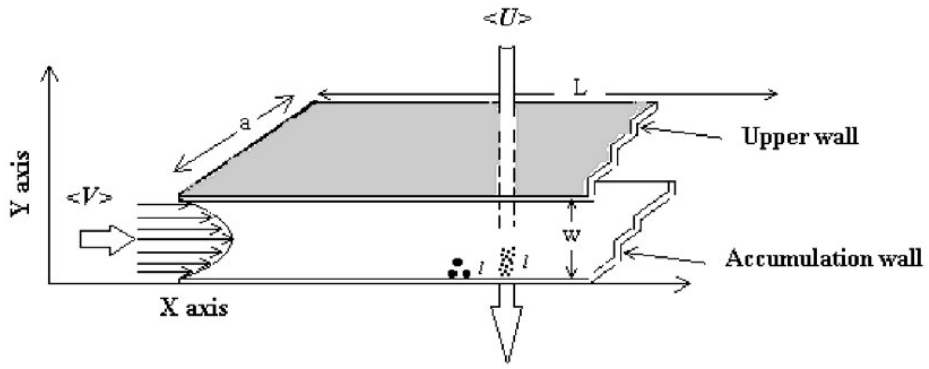

Figure 2. *Schematic flow diagram in FFF separation channel.*

Equation 5 illustrates how the layer thickness (l) can be considered as a balance between the two effects: the diffusion that increases l and the field that reduces l. Since particles of different size have different D values, they are expected to have unique l values as well. The velocity can be expressed as $<U> = F/f$, where F is the force exerted by the field and f the friction coefficient for motion of the particle in the carrier. According to the Stokes-Einstein law,

$$D = \frac{kT}{f} \tag{6}$$

where kT is the thermal energy (k = Boltzmann coefficient and T = the absolute temperature). Combining the aforementioned facts with Equation 5 leads to $l = kT/F$.

For theoretical purposes it is useful to consider *l* as part of a dimensionless retention parameter λ, as given by:

$$\lambda = \frac{l}{w} = \frac{D}{\langle U \rangle w} = \frac{kT}{Fw} \tag{7}$$

where *w* is the a channel thickness.

After the relaxation step in which the channel flow usually is stopped, the flow is redirected through the channel. This is the start of the separation process. Once again the separation process starts. Due to the parabolic flow profile, particles will migrate through the channel differentially according to their distance from the accumulation wall. Smaller particles, which are located in the middle of the channel where the flow is faster, are eluted earlier. Larger particles are relatively compressed near the accumulation wall and thus are eluted later. In consequence, smaller particles come out from the channel earlier than larger particles. The retention ratio *R*, which is the ratio of the migration velocity of any given particle relative to the mean velocity of the channel fluid-flow, is dependent on the retention parameter λ, according to:

$$R = 6\lambda\left[\coth\left(\frac{1}{2\lambda}\right) - 2\lambda\right] \tag{8}$$

When λ approaches zero

$$\lim_{\lambda \to 0} R = 6\lambda \tag{9}$$

The parameter λ is critical in all FFF subtechniques and, although it is not directly accessible experimentally, it can be related to the retention ratio *R*. *R* is the ratio of the retention time (or volume) of an unretained solute to the retention time (or volume) of the retained solute, as given by:

$$R = \frac{t^0}{t_r} = \frac{V^0}{V_r} = 6\lambda \tag{10}$$

However, when the particle size increases beyond a certain limit (approximately one micrometer), the particle radius *r* becomes greater than the ideal layer thickness *l*. Therefore Brownian motion becomes negligible and the external field holds particles firmly against the

wall. The separation process is inverted *i.e.* bigger particles emerge for detection before the smaller ones. The first mode of operation, which is affected by Brownian motion, is the normal mode, whereas the second case is referred to as a steric or hyperlayer mode.

2.1. Sedimentation FFF

Sedimentation FFF (SdFFF) was designed independently by Giddings [49], and by Berg and Bruce [50] and has proved very useful for the separation of sub-micrometer and micrometer particles. The force field used in sedimentation FFF is based on either the Earth's gravity or a centrifugal force. Figure 3A shows basic components and separation principles of SdFFF, where a flat channel (a stainless steel spacer) is coiled to form a ring within a centrifuge basket [51-53]. The sample is introduced into the channel through a septum or injection valve, and then the flow is turned off. A centrifugal field is applied at right angle and upon spinning the force pushes all particles to the outer region of the channel, *i.e.* closer to the accumulation wall (Figure 3B). There, the particles form steady-state clouds in which the field-induced migration towards the accumulation wall is then balanced by the action of diffusion away from the wall, forming a cloud layer with a characteristic thickness for all particles of a particular size (See Figure 3). The force exerted on the particles with mass m_p, density ρ_p, and hydrodynamic diameter d_H, is expressed as:

$$F = m_p \omega^2 r(1-\rho/\rho_p) = \frac{\pi}{6}\omega^2 r d_H^3 \Delta\rho \qquad (11)$$

where ρ is the carrier density, ω is the centrifuge speed (radian s^{-1}), r is the centrifuge radius, $\Delta\rho$ is the density difference between the particle and the carrier liquid. $\omega^2 r$ is the field strength expressed as acceleration. When Equation 11 is substituted in to Equation 7, a well-known relationship between λ and particle mass (m_p) or hydrodynamic diameter d_H is obtained as:

$$\lambda = \frac{kT}{m_p \omega^2 r w(1-\rho/\rho_p)} = \frac{6kT}{\pi\omega^2 r w d_H^3 \Delta\rho} \qquad (12)$$

Separation of particles is subsequently produced when the carrier flow resumes, transporting sample components at different velocities according to the mean positions of the sample clouds within the laminar flow of the carrier fluid.

The retention time (t_r) is used to determine the equivalent hydrodynamic diameter (d_H). In the case of constant field conditions for well-retained samples, the approximate expression is [54,55]:

$$d_H \approx \sqrt[3]{\frac{36kTt_r}{\pi\omega^2 rw\Delta\rho t^0}} \qquad (13)$$

Thus particles with larger mass or density have longer retention times than smaller or less dense particles. This method has been used to fractionate and determine the particle size and molar mass distributions of numerous industrial products, including carbon black [56], silica particles [57 - 59], pigments, metal and ceramic particles [60], clay [61,62] latexes [63 - 65], water soluble polymers [58,59], environmental colloids and biological macromolecules [66-69]. It also has advantages in determining the mass of adsorbed materials [70 - 72].

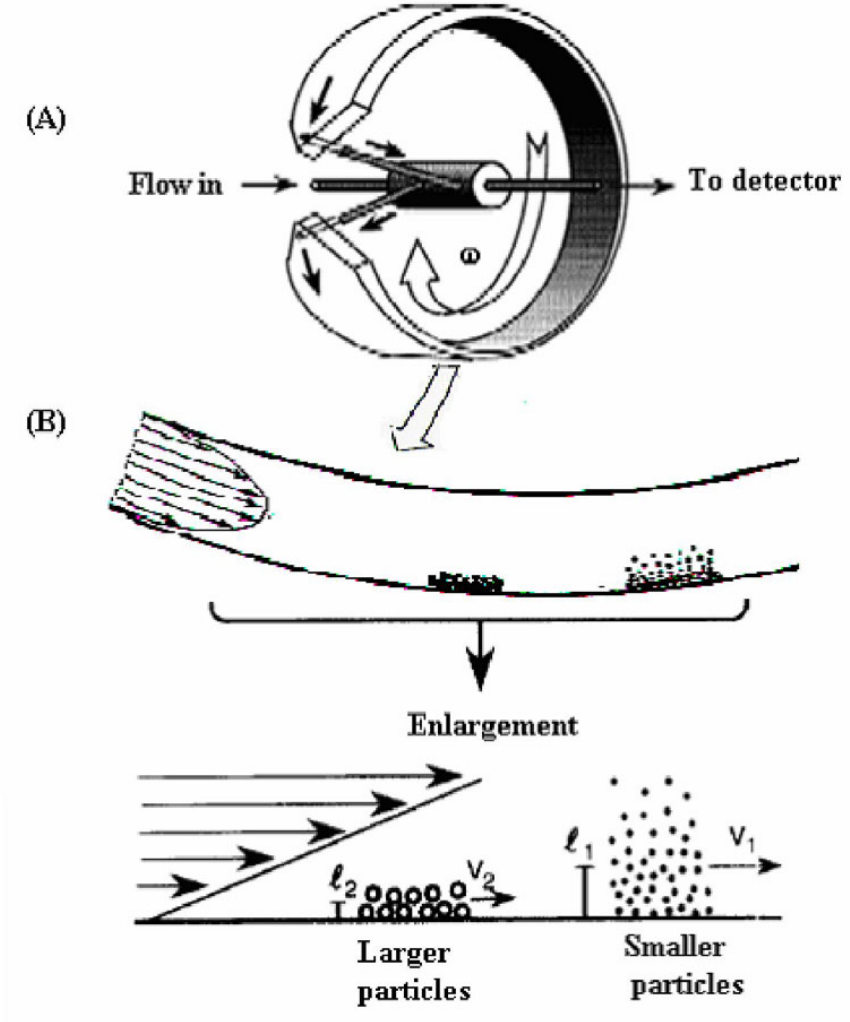

Figure 3. *(A) Schematic representation of the sedimentation field-flow fractionation apparatus. (B) Particles undergoing differential flow transportation. Reprinted with kind permission of [51] Copyright (1993) AAAS.*

2.2. Thermal FFF

Thermal field-flow fractionation (ThFFF) is a sub-technique that is favored for separation and characterization of polymeric materials where the materials can be dissolved in organic solvents. In 1967, Thompson *et al.* [73] described in detail the first design for a ThFFF channel, and the first industrial application was reported in 1969 [74]. Subsequently in 1976 Giddings *et al.* extended the technique by improving the channel structure and speeding up separations [75]. The design shown in Figure 4A is usually composed of two metallic blocks (with high thermal conductivity, preferably copper with highly polished, even surfaces) between which a spacer is clamped. The lower wall is cooled by water circulation and the upper wall is electrically heated with an electronic control circuit to maintain the desired temperature difference between the walls. Inlet and outlet capillaries are placed in the upper heated block. The sample is injected with a micro syringe through a septum or by using an injection valve. The channel shape is precisely cut into a spacer of low-thermal-conductivity material, which is then inserted between the metal blocks. The actual dimensions of the separation channel are 30-50 cm in length, 1-3 cm in width with a thickness of 0.01-0.025 cm.

The separation is based on the fact that, as shown in Figure 4B, macromolecules tend to move from the hot region towards the cold wall by thermal diffusion and this movement is eventually balanced by normal diffusion as the concentration gradient builds up. In ThFFF, the velocity $\langle U \rangle$, induced by the temperature gradient across the channel (dT/dx), is given by $D_T(dT/dx)$, where D_T denotes the thermal diffusion coefficient of the sample molecule in the carrier. The dimensionless retention parameter λ for ThFFF is given by:

$$\lambda = \frac{D}{wD_T(dT/d_x)} = \frac{D}{D_T \Delta T} \qquad (14)$$

where ΔT has replaced wdT/dx and is the temperature difference across the channel thickness, and D and D_T are normal and thermal diffusion coefficients, respectively. If l is small, the retention ratio (R) can then be expressed as:

$$R = \frac{t^0}{t_r} \approx 6\frac{D}{D_T \Delta T} \qquad (15)$$

where t^0 is the void time and t_r is the analyte retention time. Equation 15 shows that the retention time in ThFFF increases with D_T/D. The field strength can be appropriately adjusted in order to analyze samples within a broad molar mass range. In programmed ThFFF, the field strength is gradually decreased according to a temperature program to prevent excessive retention of high-molar components of broad molar mass distribution samples [76,77]. ThFFF is now widely used as an analytical separation method to determine the molar mass (M) of particles of various origins and sizes, especially of high or even ultrahigh M polymers from synthetic and natural macromolecules [78 - 80].

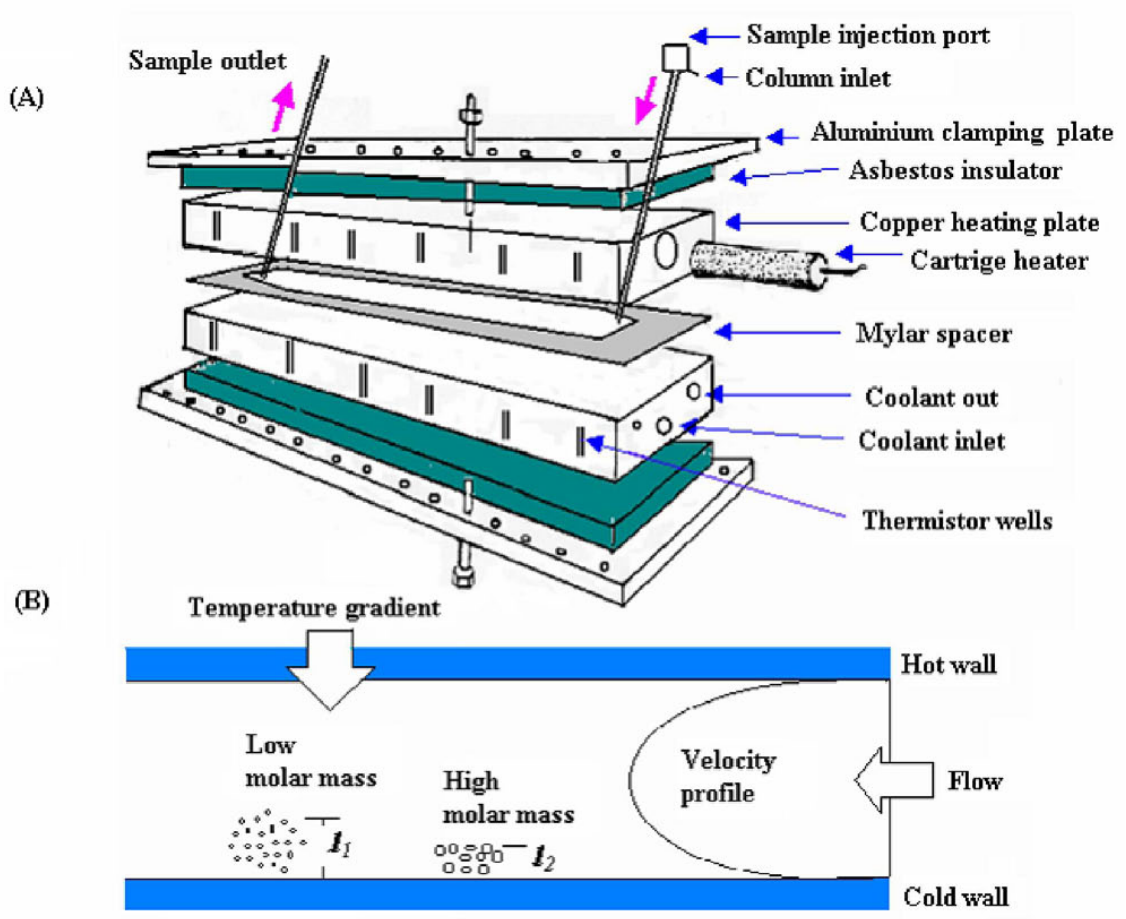

Figure 4. *Schematic representation of thermal FFF. (A) Components of the channel and (B) Polymers undergoing differential flow transport from [53] reprint with kind permission of Wiley-VCH Verlag GmbH & Co. KGaA.*

2.3. Electrical FFF

Electrical field-flow fractionation (ElFFF) was introduced in 1972 as a promising method for separation of proteins [81]. The first operational channel in ElFFF consisted of a Mylar spacer

with a cut out, sandwiched between two semi-permeable, flexible membranes. The channel was placed between two electrodes, one positive and the other one negative. Retention depended on the size and surface charge density of the sample particle. However, both retention and resolution fell short of theoretical prediction. In 1993, a new channel, designed by Caldwell and Gao, utilized two graphite plates (which served as the channel wall and electrode) separated by a Mylar spacer, which was designed to be easy to assemble and operate [82, 83], (Figure 5A).

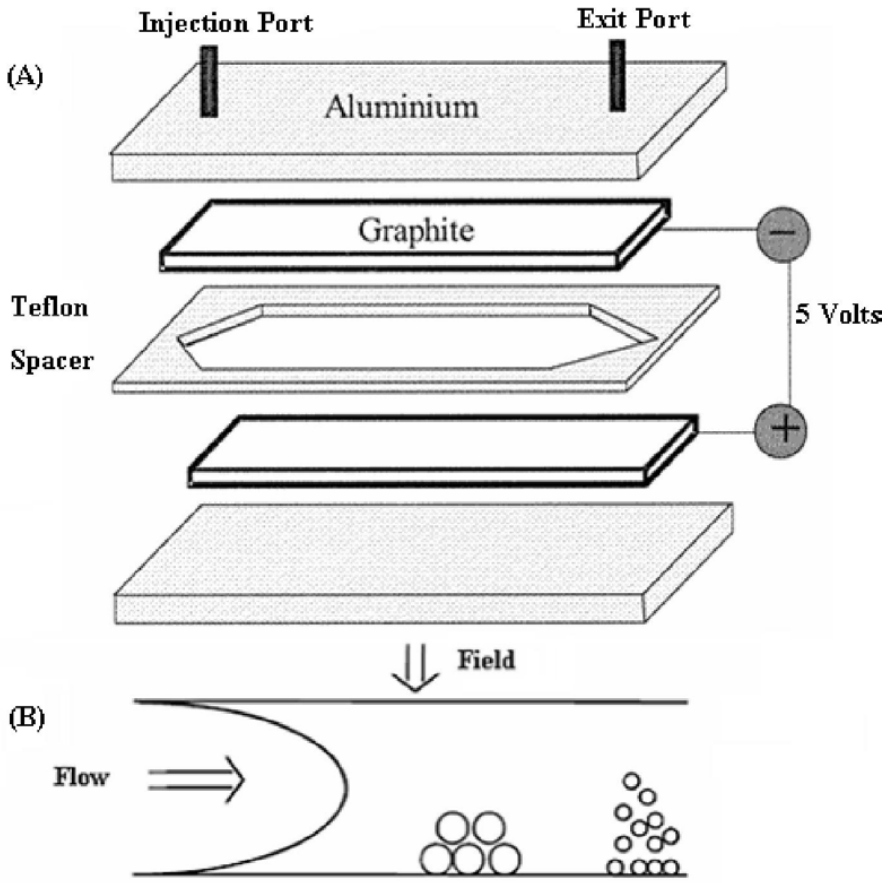

Figure 5. *Schematic of (A) an electrical FFF channel Two graphite plates serve the dual role of channel wall and electrode. Reprinted with permission from [83] Copyright © 2000 American Chemical Society; and (B) particles undergoing differential flow transport.*

In ElFFF, l is related to the magnitude of the voltage drop ΔV applied across the channel and to the hydrodynamic diameter (d_H) and electrophoretic mobility (μ) of the particles according to:

$$\lambda = \frac{l}{w} = \frac{kT}{3\pi\eta} \times \frac{1}{\mu d} \times \frac{1}{\Delta V} \qquad (16)$$

The main application of ElFFF systems has been for serration and particle size characterization of proteins and latex materials (Figure 5B). Over the last few years, however, great effort has been devoted to the development of micro scale total analysis systems (μ-TAS), which integrate sample handling, analysis, detection, and signal processing. The main component of many μ-TAS setups is supposed to be a chromatograph in which the analysis is to be performed. Another approach of significant interest that has been reported is the micro machined electrical field-flow fractionation (μ-ElFFF) system. This miniaturized electrical FFF, fabricated on a microchip, is intended for separation of biological particles, including blood proteins, DNA, liposomes, organelles, viruses, and polymers, and it is meant for use in biochemistry, cell biology, bioengineering, and pharmaceuticals [84-86].

2.4. Flow FFF

Flow field-flow fractionation (FlFFF) was introduced in 1976. This technique has since proved to be the most universal and most frequently used of all FFF techniques [87, 88]. The universality comes from the fact that the technique employs a hydrodynamic field applied by means of a cross flow perpendicular to the main flow [89]. Specifically, pumping a bulk liquid into the channel through one of the porous walls creates a convective flux. The liquid then exits the channel through the opposite wall, the so called “accumulation wall”, that consists of an ultrafiltration membrane placed on the top of a porous wall. For this reason, retention time in FlFFF is, in principle, dependent on diffusive flux, and separation of macromolecules or particles occurs solely on the basis of differences in diffusion coefficients [90]. In FlFFF, almost any liquid solution can be used as mobile phase and its selectivity, in terms of differences in diffusion coefficients, is particularly high.

There are two types of flow FFF, one of which is a symmetrical flow FFF, and the other, which is an asymmetrical flow FFF. The symmetrical flow FFF, as shown in Figure 6A, consists of upper and lowers semi-permeable porous frits within Plexiglas blocks. The cross flow vector is thereby created by pumping a secondary liquid into the channel through one of the wall with an equal amount of flow seeping out through the accumulation wall. The accumulation wall has a well-defined molar mass cut-off, due to the presence of an ultrafiltration membrane which is permeable to the solvent but not to the macromolecules.

Because small molecules like salts and many contaminants are usually flushed through the membrane, they do not disturb the detection of actual sample. Two or three different modes of operation can be used within the same channel, namely normal and steric/hyperlayer operational modes.

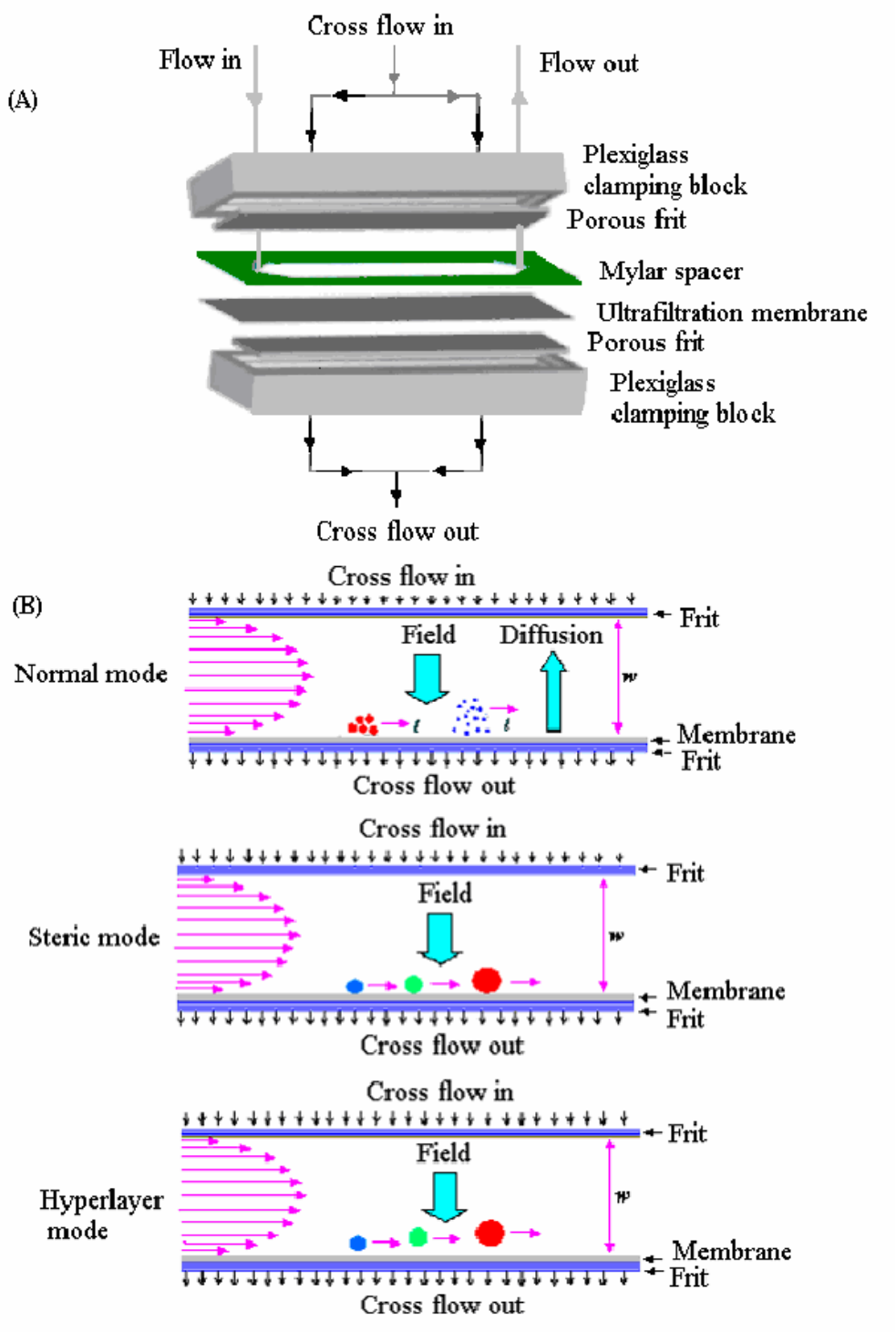

Figure 6. *The separation channel of flow field-flow fractionation in (A) and separation modes of samples in (B).*

2.4.1. Normal (Brownian) mode

In the normal mode of FlFFF, separation of particles is based on two simple steps (Figure 6B). After sample injection, the sample components are carried by the cross flow towards the accumulation wall. The field is opposed by diffusion, which leads to formation of a narrow exponential concentration distribution or layer of unique thickness (*l*). This layer thickness, *l*, is the ratio of the diffusion coefficient (*D*) to the external drag induced by the velocity $\langle U \rangle$ as explained earlier in Equation 7. The field strength due to $\langle U \rangle$ in Figure 2 can be related to the volumetric flow rate of the cross flow divided by the area of the channel [87], as given by:

$$\langle U \rangle = \frac{\dot{V}_c}{aL} \tag{17}$$

where *a* is the width and *L* is the length of the channel. The velocity $\langle U \rangle$ is equal for all particles independently of their size because it originates from the flowing bulk fluid. The rate of transport by diffusion, however, is different for every particle depending on its diffusion coefficient (*D*) [91]. The dimensionless retention parameter λ for FlFFF is related to *D*, channel void volume V^0, cross flow rate $\dot{V}_c$, and the channel thickness, *w* by:

$$\lambda = \frac{l}{w} = \frac{D}{w\langle U \rangle} = \frac{DaL}{w\dot{V}_c} = \frac{DV^0}{w^2\dot{V}_c} \tag{18}$$

In Equation 18, V^0 and *w* are constants from the physical geometry of the channel, and $\dot{V}_c$ is measurable using a volumetric flow rate. Separation of different particle zones in the channel is therefore based solely on the differences in diffusion coefficient of the particles [88]. As for the other FFF subtechniques, the retention parameter λ, is related to the retention ratio *R* from Equation 10. The retention time of samples can be obtained by inserting λ from Equation 18 into Equation 10, as given by:

$$R = \frac{t^0}{t_r} = 6\left(\frac{DV^0}{w^2\dot{V}_c}\right) \tag{19}$$

where *R* is the ratio of the retention time or volume of an unretained solute to the retention time of the retained solute.

The experimental particle size in flow FFF can be obtained from the retention time by combining Equations 1 and 19 as:

$$d_H = \frac{2kTV^0}{\pi\eta w^2 \dot{V}_c} \frac{t_R}{t^0} \qquad (20)$$

Smaller species appear first and larger ones come out last, because small particles generally have larger *D* values than large particles. Equation 20 can be used either to determine the particle size of analytes, or the channel thickness *w* by back-calculation from the retention time of standard materials with known hydrodynamic particle sizes.

2.4.2. Steric/hyperlayer mode

When particle sizes increase beyond a certain limit (typically approximately one micrometer), Brownian motion becomes negligible. In an idealized model of steric FFF, particles touch the accumulation wall and the external field holds particles firmly against the wall (Figure 6B). In this case, the particles are still displaced by the flow stream but their velocity depends on how far they protrude out into the channel. Larger particles extend further into the fast streamline regions of the channel than do the smaller particles. Thus in this so-called steric mode, as opposed to the normal mode, the larger particles emerge first, followed by successively smaller particles [92, 93]. However, the idealized model of steric FFF is affected by hydrodynamic lift force, which tends to pull the particles away from direct contact with the accumulation wall. The opposing cross flow force and lift force drive these particles into bands (or hyperlayers) elevated some distance above the accumulation wall, giving rise to the hyperlayer mode. The hyperlayer is formed at a point where the two opposing forces (the cross flow and hydrodynamic lift) are equal. Large particles equilibrate farther from the accumulation wall than smaller particles and thus larger particles emerge first in the elution sequence. With a sufficiently thin hyperlayer, non-equilibrium band broadening is less significant in the hyperlayer mode, than in the normal mode. Fast flow rates can be used in the steric/hyperlayer mode to achieve high-speed separation and to minimize band spreading. This is a major advantage of steric-hyperlayer over normal mode separations.

The retention ratio (R) in steric mode is approximated as:

$$R = \frac{6\gamma}{w} r_H = \frac{3\gamma}{w} d_H \qquad (21)$$

where r_H and d_H are the hydrodynamic radius and hydrodynamic diameter of the particle, and γ is a correction factor that accounts for various non-ideal phenomena, such as hydrodynamic lift forces and frictional retardation due to interactions with the accumulation wall, or any other possible perturbations. For steric/hyperlayer FlFFF, γ is of the order of unity. However, it varies with particle diameter, flow rate and other parameters due to the influence of the hydrodynamic effect.

A calibration plot with the logarithm of retention time versus logarithm of particle diameter gives a convenient means for obtaining the particle size distribution of spherical or near-spherical particles. The calibration curve yields a straight line, which can be expressed by:

$$\log t_r = -S_d \log d_H + \log t_{r1} \qquad (22)$$

where S_d is the negative slope of the plot, expressed as the size or diameter selectivity, and t_{r_1} is a constant. From the calibration parameters S_d and t_{r_1}, the particle size distribution for an unknown sample can be obtained using the above equation.

2.4.3. Asymmetrical flow FFF

The asymmetrical version of flow FFF (AsFlFFF) was first introduced in 1986 [94, 95] and further developed in the late eighties and the beginning of the nineties [43, 44, 96- 98].

In AsFlFFF only one wall element is permeable to the flow, in contrast to FlFFF, where two permeable walls are needed (Figure 7A). The incoming flow from the AsFlFFF channel inlet is divided into two components, namely the main flow (axial component) and the cross flow (perpendicular to the main flow), whereas in symmetrical FlFFF these two flows go into the channel separately. Figure 7B illustrates a simple, enlarged side view across the channel thickness (w). The retention mechanisms are similar to symmetrical FlFFF and the normal,

steric and hyperlayer modes can be equally applied in both normal FlFFF (Figure 6B) and AsFlFFF (Figure 7B).

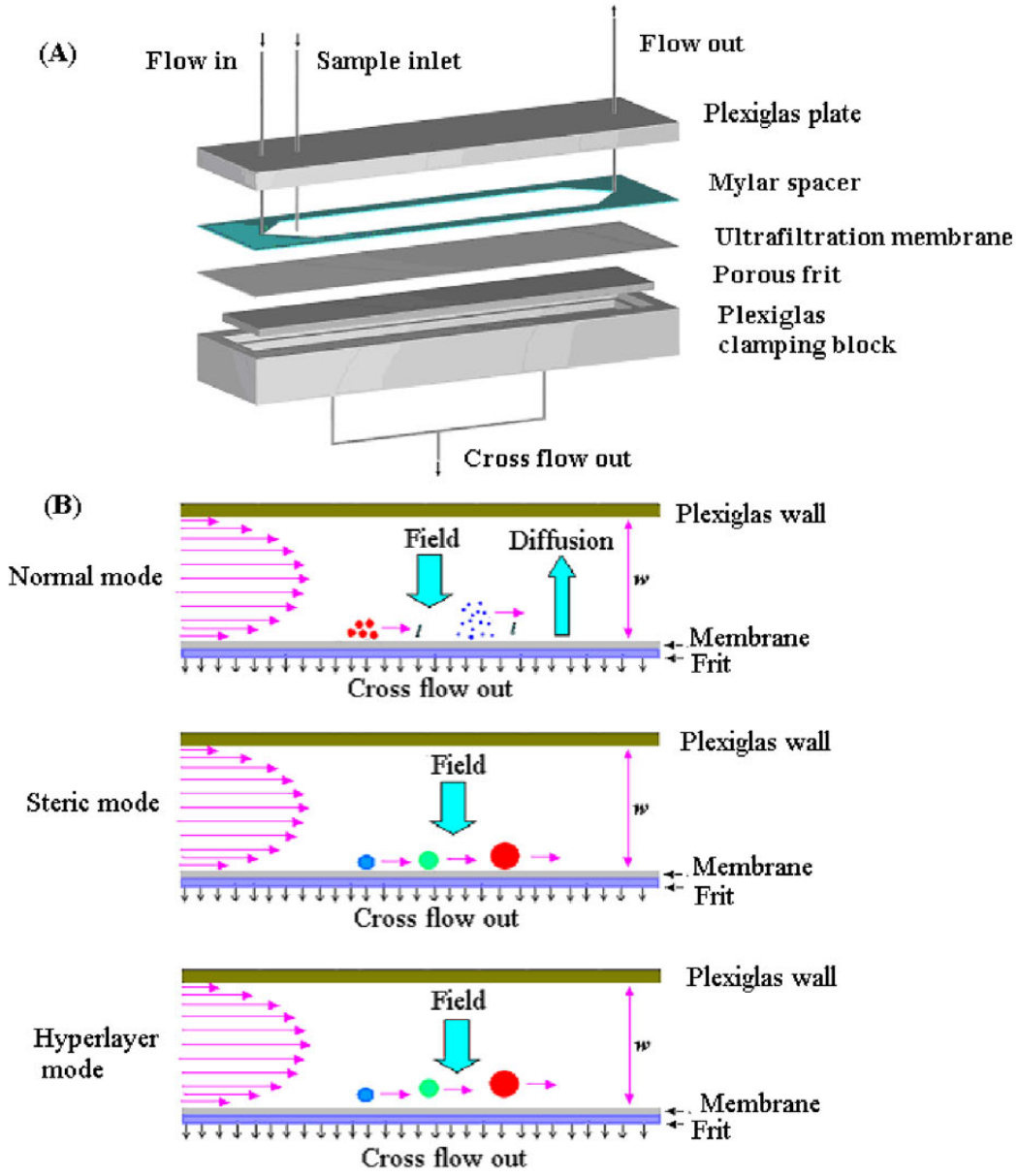

Figure 7. *The separation channel of asymmetrical flow field-flow fractionation in (A) from [99] reprint with kind permission of Springer Science and Business Media; and separation of samples in (B).*

In symmetrical FFF, stop flow is used during the relaxation period to let the particles find their equilibrium positions before the run is started. This is accomplished by turning off the main channel flow and, at the same time, the external field is applied just long enough to

pump about one channel volume (V^0) of cross flow. Because the flow in asymmetrical FlFFF cannot be stopped independently of the field, a different approach, called opposing flow relaxation, is applied in combination with sample injection at a separate inlet (Figure 8A) a few centimeters downstream from the inlet. The relaxation process is then achieved for both rectangular and trapezoidal channels allowing the carrier liquid to flow in from both the inlet and outlet of the channel and meet at one point, the so-called focusing point (Figure 8B). The focusing action of the two flow streams plays an important role in reducing bandwidth, as well as achieving successful sample relaxation. The sample, no matter where it was loaded or how widely it was dispersed, will eventually migrate and become focused and relaxed on a narrow zone at this junction point. According to Equation 23, altering the two opposing flow rates can lead to a shift of the focusing position (z'):

$$\frac{z'}{L} = \frac{\dot{V}_{inlet}}{(\dot{V}_{inlet} + \dot{V}_{outlet})} \qquad (23)$$

where z' is the focusing position of the analytes from the inlet of the channel, L is the length of the channel, and $\dot{V}_{inlet}$ and $\dot{V}_{outlet}$ are the flow rates from the inlet and outlet respectively.

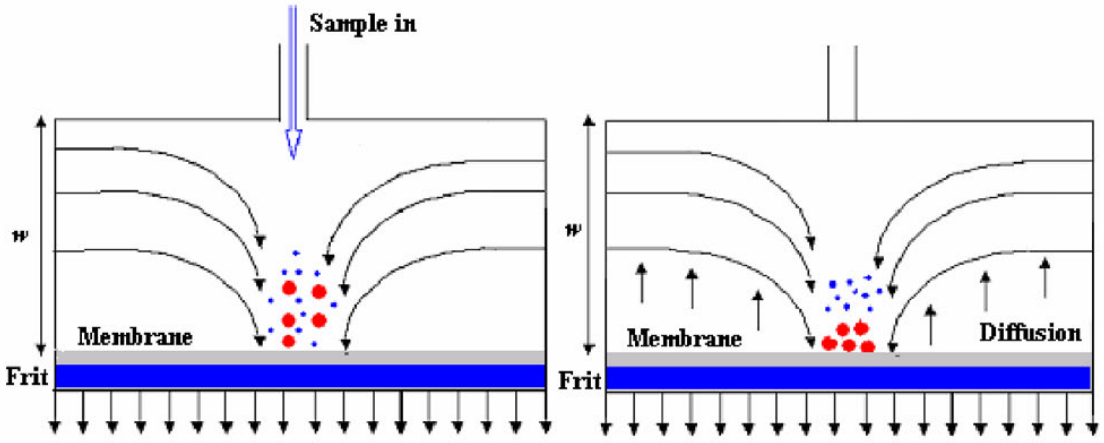

Figure 8. *(A) Sample injections in AsFlFFF. (B) Focusing/relaxation in AsFlFFF.*

The asymmetrical Flow FFF system has a number of advantages over the symmetrical system: (i) the construction is technically simpler; (ii) the effect of heterogeneity and the possibility of uneven permeability of the upper frit of the symmetrical channel as well as the

non-uniformity of its surface is eliminated in the asymmetrical system; (iii) through the glass wall of the asymmetrical channel, it is possible to observe the migration of suitable samples; and (iv) samples can be concentrated on-line using the asymmetrical system. On-line concentration might not be so easily achieved with symmetrical FlFFF.

FlFFF and its variant AsFlFFF have been used to fractionate and determine the particle size and molar mass distributions of synthetic polymers soluble in aqueous or organic solvents [79, 100 - 106]; biopolymers, including proteins (bovine serum albumin, β-lacto globulin, γ-globulin, thyroglobulin, ferritin, ribonuclease, and hemoglobin) [43, 44, 90, 107, 108], lipoproteins from blood plasma [45], casein micelles from milk and milk products [109, 110], wheat proteins [111, 112], DNA [43, 48, 113], liposomes (lipid vesicles) [47, 114, 115], ribosomes [5, 116, 117] and pullulans; latex materials used in the coating industry [107, 118 - 121]; environmental humic substances and humic related particulates [122 - 131], and aggregates of particles [132]

2.4.4. Hollow fiber flow FFF

Hollow fiber flow FFF (HF FlFFF) is carried out in a cylindrical tube made up of a semi-permeable (ceramic) fiber contained in an open metal or a glass tube, in contrast to the normal FlFFF, which needs two parallel plates [133, 134]. The separation steps are quite similar to those for asymmetrical FlFFF; that is, injection, relaxation focusing and elution steps. Molecules are forced towards the inner wall of the hollow fiber by a cross-flow, which pushes the liquid through the pores of the channel. Depending on their size, molecules are distributed over different velocity lines of the axial flow, and are thereby separated by size. What is most important about this method is that analysis can be made using both aqueous and organic solvents. The method is also suitable for macromolecules of *ca.* 2000 Da up to particles of 100 μm. The basic principle of HF FlFFF is shown in Figure 9.

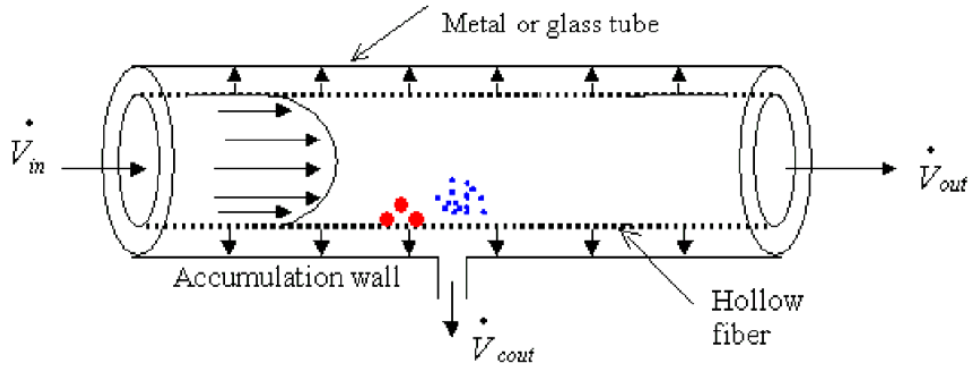

Figure 9. *Principle of hollow fiber flow FFF.*

2.4.5. Determination of void volume and channel thickness

The void volume V^0, or the void time t^0, are essential parameters that must be determined before the particle size can be calculated. Physically, the void volume can be interpreted as the geometrical volume of the free space in the channel, that is, it can be calculated from the width, length and thickness if they are known accurately ($V^o=aLw$). However, the channel thickness may slightly vary from time to time when the channel is opened and reassembled again. Giddings *et al.* in 1992 [135] described a peak break-through method for measuring the void volume. When a high molar mass compound is passed through the channel, without any cross flow or relaxation, the first probe molecules to appear are those which travel at the center of the channel. When the average fluid flow rate is considered as F_r, the flow rate at the center (F_{rc}) of the channel would be 1.5 times that of the average fluid flow rate. That is:

$$F_{rc} = 1.5 \times F_r \qquad (24)$$

where F_{rc} is the flow rate for the first break-through profile. Equation 24 shows that the flow rate of the fastest probe molecules is 1.5 times faster than the average fluid flow, and the average time (the void time) is 1.5 times longer than the break-through time (t_{br}). Thus:

$$t^0 = 1.5 \times t_{br} \qquad (25)$$

Similarly, in view of the proportionality between time and volume, the measured break-through volume V_{br} can be related to the average volume V^0 (void volume) according to:

$$V^0 = 1.5 \times V_{br} \qquad (26)$$

Therefore, the measurement of t_{br} and V_{br} leads directly to the corresponding void parameters t^o and V^o.

Ideally, the void time t^0 can be obtained as an elution time of unretained component, which travels with the average velocity $\langle V \rangle$ of the carrier. In AsFlFFF, this void time is dependent on the axial flow rate similarly to other forms of FFF, but it is also dependent on the cross flow rate, which affects the location where the sample is focused before the separation is started. Instead the void time (t^0) has to be defined as a function of void volume, axial flow rate and cross flow rate using Equations 27-29:

$$t^0 = \frac{V^0}{\dot{V}_c} \ln\left\{1 + \frac{\dot{V}_c}{\dot{V}}\left[1 - \frac{w\left(a_0 z' - \frac{(a_0 - a_L)}{2L} z'^2 - y'\right)}{V^0}\right]\right\} \tag{27}$$

where z' is the distance from the inlet to the focusing point, L is the channel tip-to-tip length, y' is the area cut off (reduction) of the accumulation wall due to the tapered channel inlet, and a_0 and a_L are the channel width at the inlet and outlet, respectively. For a rectangular (a_0=a_L) or trapezoidal channel, a more simplified form of Equation 27 can be written as follows:

$$t^0 = \frac{V^0}{\dot{V}_c} \ln\left[1 + \frac{\dot{V}_c}{\dot{V}}\left(1 - \frac{A(z') - y'}{A_{total}}\right)\right] \tag{28}$$

with A_{total} being the area of the accumulation wall and $A(z')$ corresponds to the uncorrected area of the wall from the channel inlet to the focusing point. At a focusing point z', around the sample introduction port, the difference between $A(z')$ and y' over the total area approaches zero, so that Equation 28 can be reduced to give:

$$t^0 = \frac{V^0}{\dot{V}_c} \ln\left(1 + \frac{\dot{V}_c}{\dot{V}}\right) \tag{29}$$

where $\dot{V}$ is the channel flow rate.

Spacer thickness measurement by micrometer can be used to estimate the value of channel thickness *w* but does not usually give accurate results since the accumulation wall membrane protrudes somewhat into the channel and the actual channel is thinner than the nominal spacer thickness. The most convenient method to determine *w* is to use the retention time of standard materials with known diffusion coefficients or hydrodynamic particle sizes. This allows *w* to be calculated using the fundamental relationship between the experimental retention time and the diffusion coefficient (Equation 19).

2.4.6. Band broadening and resolution

Particles in FFF systems are not generally limited to the volume into which they were initially injected, but they tend to become dispersed across the channel by mixing, diffusion, and other forces. As these particles spread in the channel, they begin to overlap and cause a loss of separation efficiency.

As in chromatographic techniques, band broadening in FFF can be discussed in terms of plate height, *H*, which is a fundamental parameter related to various properties of the particles and the FFF device via the relationship [98, 136 -138]:

$$H = \frac{2D}{R\langle V \rangle} + \frac{\chi w^2 \langle V \rangle}{D} + \sum_i H_i + H_p \qquad (30)$$

where D is the diffusion coefficient of the particles, $\langle V \rangle$ is the average fluid velocity through the FFF channel, and χ is a non-equilibrium dimensionless parameter. In equation 30, the first term represents the contribution of the longitudinal diffusion and is generally negligible, because most analytes have high molar mass or size and consequently have a small diffusion coefficient. The second term is the contribution of non-equilibrium effect (H_n), caused by the inherent distribution of the sample through out the channel. χ is a complicated function of λ. If λ is small, the approximation $\chi=24\ \lambda^3$ can be used [139, 140]. The third term is the sum of instrumental contributions (H_i) such as injection, detection, system dead volume, and flow irregularities [141 - 143].

For a well-constructed FFF apparatus that is being properly operated, the third term will also be small. The fourth term H_p is the contribution of particle size polydispersity to the plate height [136], as given by:

$$H_p = L\left(\frac{d \ln R}{d \ln \lambda}\right)^2 \left(\frac{\sigma_d}{d}\right)^2 \tag{31}$$

where σ_d is the standard deviation of the particle size distribution, d is the mean diameter (d_{mean}), and L is the channel length. When λ approaches zero, the value of H_p is given in a reduced form as [138]:

$$H_p = L\left(\frac{\sigma_d}{d}\right)^2 S_d{}^2 \tag{32}$$

where S_d is termed the diameter-based selectivity. For highly retained samples in FlFFF, S_d is 1 and in SdFFFF, it is 3, which gives SdFFF more separation power per unit diameter than FlFFF. Band-broadening contributions can be expressed in terms of the increment in the time-based variance, σ_t^2. If the contributing σ_t^2 is known, then the unwanted increase in the plate height H can be calculated using [144]:

$$H = \frac{\sigma^2{}_t}{t_r^{\,2}} L \tag{33}$$

where σ_t^2 is the variance of an FlFFF peak in time units, and t_r is the retention time. Thus the plate height can be determined from experimental data by measuring the breadth of the peaks as they elute.

A common alternative representation of plate height is the number of theoretical plates, N. The value N is equal to L/H. From data, N can be calculated as follows [145]:

$$N = 5.54\left(\frac{t_r}{w_{1/2}}\right)^2 = \frac{L}{H} \tag{34}$$

The most important index of success for the analytical separation of two specific components is the resolution R_s. This parameter categorizes the overlap of two specific component zones.

If the centers of gravity of the two zones are found at locations X_1 and X_2, respectively, then the resolution can be defined as [146]:

$$R_s = \frac{2(X_2 - X_1)}{W_{b1} + W_{b2}} \tag{35}$$

where X is the peak retention time or volume; W_b is the peak width formed by the intersection of the tangents to the curve inflection points with the baseline in retention volume units, $W_b = 4\sigma$ and σ is the peak standard deviation (proportional to peak width). The subscripts 1 and 2 serve to identify two closely eluting solutes.

3. AIM OF THE STUDY

The main objective of the study was to exploit asymmetrical flow field-flow fractionation for studies of particle sizes, molar masses, and aggregate formation of macromolecules. Special emphasis was put on determining the effect of several parameters such as pH, ionic strength, temperature and reactant mixing ratios. The specific aims were:

1. To study the effect of hydrophobic and electrostatic interactions on protein-lipid complex formation (I).
2. To apply AsFlFFF to the determination of the volume phase transition of thermosensitive polymers, as well as aggregate particle sizes, after thermally induced changes (II).
3. To study the effect of salt and the molar ratio of polycations and polyanions on polymeric complex formations (III).
4. To monitor physical or chemical instabilities affecting the shelf life of liposomes (IV).
5. To study the effect of pH, ionic strength, vortexing, and chemical and enzymatic treatments on the sizes of low-density lipoprotein particles (V).
6. To construct a miniaturized asymmetrical flow field-flow fractionation system and to compare its operation to that of conventional asymmetrical flow field-flow fractionation in protein studies (V).

4. MATERIALS AND EXPERIMENTAL METHODS

A general overview of the materials and methods is given below. More details are presented in the original publications (I –V).

4.1. Materials

Poly-N-isopropylacrylamide-(PNIPAM),poly-(methacryloxyethyl trimethylammonium chloride, (PMOTAC)), poly (ethylene oxide)-block-poly (sodium methacrylate, (PEO-b-PMAA)) and polyelectrolyte complex (PEC) polymers were synthesized in the Laboratory of Polymer Chemistry, Department of Chemistry, University of Helsinki. Polystyrene sulphonate standards (PSS) were purchased from Scientific Polymer Products Inc. (Dean Parkway, New York 14519, USA). Polyethylene oxide standards (PEO) were purchased from Polymer laboratories Ltd., UK. Cytochrome c (cyt c, MW 12.4 kDa) was obtained from Santen Oy (Tampere, Finland). Chymotrypsinogen A (MW 25.6 kDa), bovine serum albumin (BSA, MW 66.43 kDa, 98% purity, remainder mostly globulins), transferrin (MW 79.55 kDa), catalase (MW 250 kDa), and SDS (MW 288.4) were from Sigma (St. Louis, MO, USA). According to the manufacturer, BSA contains 2% γ-globulin (MW of 155–160 kDa). Ferritin (MW 440 kDa) and thyroglobulin (MW 669 kDa, purity 95%) were purchased from Pharmacia (Amersham Biosciences, Little Chalfont, Buckinghamshire, England). 1,2-dimyristoyl-*sn*-glycero-3-[phospho-*rac*-(1-glycerol)] (sodium salt) (DMPG), egg yolk phosphatidylcholine (PC), egg yolk monosodium salt l-α-phosphatidic acid (PA), egg yolk sodium salt l-α-phosphatidyl-*dl*-glycerol (PG), and bovine liver sodium salt l-α-phosphatidyl inositol (PI) were from Avanti Polar-Lipid (Alabaster, Al, USA). Oleic acid (OA, MW 282.5, purity >96%) was obtained from KeboLab (Espoo, Finland). *N*-(2-hydroxyethyl)piperazine-*N*′-(2-ethanesulfonic acid) (HEPES), 1-palmitoyl-2-oleyl-*sn*-glycero-3-phosphatidylcholine (POPC), bovine brain phosphatidylserine (PS), cholesterol, and androstenedione were purchased from Sigma (St. Louis, MO, USA). Progesterone, testosterone, and sodium dihydrogen phosphate were purchased from Merck (Darmstadt, Germany). Sodium hydroxide (1.0 M) and hydrochloric acid (1.0 M) were from FF-Chemicals (Yli-Ii, Finland), methanol was from Mallinckrodt Baker (Deventer, The Netherlands), and chloroform was from Rathburn Chemicals (Walkerburn, Scotland). During the PNIPAM-polymers temperature effect study, the AsFlFFF separation channel was immersed in a thermostated bath.

Temperature of the bath was controlled by an electrical heater (type 01T440, Heto, Birkerod, Denmark).

4.2. Experimental techniques

4.2.1. Asymmetrical flow field-flow fractionation

The AsFlFFF channel was constructed in-house in a manner similar to that used by other groups [43, 44, 95 - 98]. The channel consisted of a porous ceramic frit placed in a Plexiglas wall. The edge of the frit was coated with cellulose acetate. For the experiments with asymmetrical FFF the upper wall of a symmetrical channel was replaced with a Plexiglas plate.

An ultrafiltration membrane, either a regenerated cellulose acetate (DSS-RC70PP, Nakskov, Denmark) or regenerated cellulose (NADIR UF-C-10) both with a molar mass cut-off of 10 kDa, was laid on top of the porous frit of the accumulation wall. A Mylar™ spacer with a thickness of 500 µm, with the channel shape cut out, was placed between the ultra filtration membrane and the upper wall. The nominal channel dimensions were 38 cm x 2 cm x 500 µm. An HPLC pump (model PU-980, JASCO International Co., Ltd., Tokyo, Japan) was used to move the carrier liquid. Applicability of a miniaturized asymmetrical flow field-flow fractionation (mAsFlFFF) channel connected to a UV/VIS detector was also tested in the separation of proteins and lipoproteins. With the geometrical channel dimensions of a conventional AsFlFFF (38cm x 2cm) scaled down to 11 cm in length and 0.7 cm - 0.35 cm in width (trapezoidal channel), the flow rate ranges could be decreased. Channel thickness (500 µm) was the same for both the conventional and miniaturized channels. A trapezoidal thick channel was chosen to decrease particle-wall interactions, and it also allowed the use of high sample concentrations to increase detection sensitivity. The outlet flow from the channel was monitored with a UV/VIS detector (HP1050 model 79853C, Tokyo, Japan) at 214, 254, 280 or 410 nm, or with a UV detector (model ISCO UA-5, Instrument specialties, Lincoln, Nebraska, USA). Capillary Teflon tubes (i.d. 0.5 mm), restrictors (from a local electrical shop), and three-way valves (V101T; Upchurch Scientific, Oak Harbor, WA, USA) were used

to control the carrier liquid flows. An Agilent ChemStation for LC and LC/MS (Palo Alto, California) was used for data acquisition.

Instrumental operations: A complete operation in AsFlFFF has three required stages. The operation starts with injection-relaxation during the first stage. Fresh carrier liquid was delivered by JASCO PU-980 (pump no. 1; Figure 10A), at 0.1 ml/min to the inlet of the channel. At the same time, the carrier liquid was delivered through the detector to the channel by air pressure. The air pressure was set to 270 - 490 kPa. As shown in Figure 10A, the liquid flow was drained off through the cross flow outlet at the bottom side of the channel (2.6-3.3 ml/min). The sample was delivered to a position 2.0 cm from the inlet by using another JASCO PU-980 (pump no. 2) at a flow rate of 0.5 ml/min to 1 ml/min, for 2-5 min. For mAsFlFFF, the sample was delivered to a position of 1.0 cm. A relaxation period of 5 to 20 minutes followed sample injection. During the relaxation period, the sample components accumulated at a particular point called the focusing point or position, as discussed in chapter 2, section 4.3.

During the second stage, as shown in Figure 10B, the run was initiated by switching the three port valve towards the main flow outlet (waste) and at the same time the main flow rate from pump no. 1 was set to a flow rate as required for particle separation. Both outlet flow rates were regulated using restrictors and measured using a flow meter, stopwatch and a burette. During the third stage, at the end of the run, the channel was rinsed for a few minutes by letting the carrier fluid flow from pump no. 1 to the outlet, while the cross flow was stationary. During this stage the tube inside of the pressurized bottle was filled with fresh buffer for the next run.

AsFlFFF using a UV detector produces a mass-weighted distribution assuming that all the particles have the same density. The mass-average (mean) diameter is calculated from the peak maximum by: $d_{mean} = \sum G(d_i) d_i / \sum G(d_i)$, where $G(d_i)$ is a probability for the fraction of particle size of d_i.

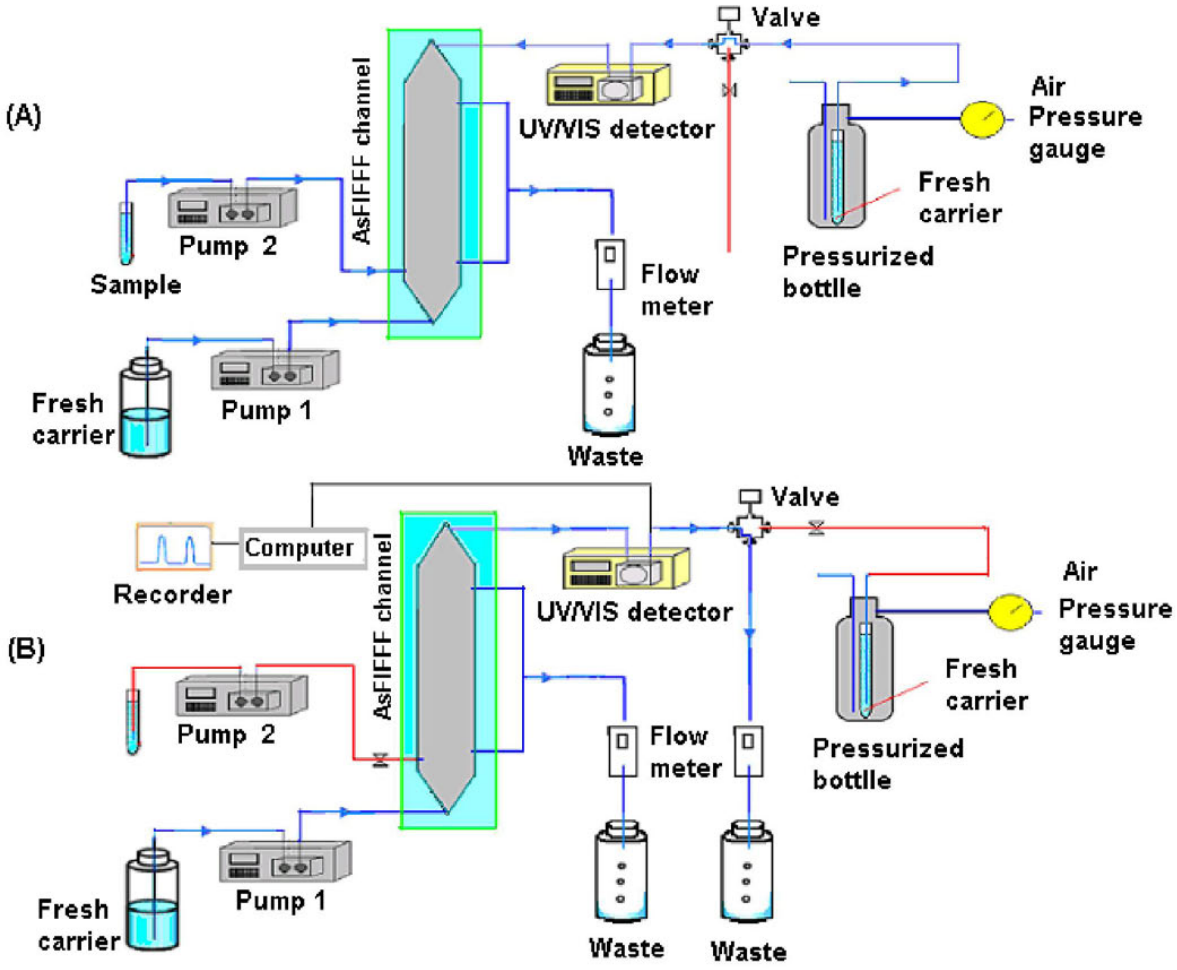

Figure 10. *AsFlFFF operational setup (A) Injection-relaxation period, (B) Elution period.*

4.2.2. Dynamic light scattering

DLS measurements were conducted at 25 ^{o}C with a Brookhaven Instruments BI-200SM goniometer and a BI-9000AT digital correlator. The light sources were a He-Ne laser (632.8 nm wavelength, power 60 mW, and angle 90^{o}), and a Lexel 85 Argon laser (514.5 nm, power range 30-150 mW and 90°), for the study of PNIPAM and PEC polymer respectively. The time correlation functions were analyzed with a Laplace inversion program (CONTIN). The samples were filtered through Millipore membranes (0.45 μm pore size) before analysis was carried out.

4.2.3. Size exclusion chromatography

In our case study, SEC was used for the study of PNIPAM and PEC polymers. The equipment (Pump 515, autosampler 717, differential Refractive index detector 2410, three Styragel packing columns HR2, HR4 and HR6 with 300 × 7.8 mm, 5 μm particle size, and one Styragel guard column) was from Waters Corp., Milford, MA, USA. The effective molar mass ranges for HR2, HR4 and HR6 were $5.0x10^2$ -$2.0x10^4$; $5.0x10^3$ - $6.0x10^5$ and $2.0x10^5$ - $1.0x10^7$ respectively. Tetrahydrofuran HPLC grade (Rathburn, Chemicals Ltd., Walkerburn Scotland) was used as an eluent and the calibration was carried out with polystyrene standards (Showa Denko, Japan). The concentration, flow rate, injection volume and temperature were 1.0 mg/ml, 0.8 ml/min, 20-100 μl, and 30 ^oC, respectively.

4.2.4. Capillary electrophoresis

Capillary electrophoresis (CE) experiment for the study of liposome coating and separation of steroids were carried out with HP ^{3D}CE equipment (Agilent, Waldbronn, Germany) with a UV diode-array detector. Separation conditions were as following: injection for 5 s at 50 mbar, separation voltage of 20 kV, temperature of capillary cassette 25 °C, and detection at 200 or 245 nm. The background electrolyte (BGE) solution was HEPES at pH 7.4 (ionic strength of 20 mM). Fused-silica capillaries from Composite Metal Services (Worcestershire, UK) with dimensions of 50 μm I.D. × 375 μm O.D were used. The length of the capillary was 40 cm to the detector (48.5 cm in total length) when egg yolk phosphatidylcholine (EPC) or EPC with calcium coatings were employed, and 60 cm (68.5 cm in total length) with EPC/PS and EPC/PS/cholesterol coatings.

4.2.5. Preparation of liposomes

The simplest way to prepare liposomes is by mechanical dispersion of the dry lipid in water. However this may result in the formation of multilamellar vesicles (MLVs), which consist of concentric bilayers separated by thin aqueous sheets. MLVs are heterogeneous systems with a large size (≥ 400 nm diameter) and relatively low entrapped aqueous volume. Unilamellar vesicles with a large trapped volume can then be obtained by either extrusion or sonication.

Unilamellar vesicles can be categorized into two classes on the basis of size. Vesicles under 50 nm in diameter are usually considered small unilamellar vesicle (SUVs), whereas those with a greater diameter are referred to as large unilamellar vesicles (LUVs). To prepare multilamellar phospholipid vesicles, appropriate amounts of the phospholipid stock solution were first dissolved in chloroform and mixed well to obtain the desired compositions. The resulting mixture was then evaporated to dryness under a stream of nitrogen, and traces of solvent were removed by evacuation under reduced pressure for 24 h. Samples were then hydrated in a buffer for 60 min at a temperature above the main transition temperature to yield multilamellar vesicles. To prepare large unilamellar phospholipid vesicles, the MLVs dispersions were subsequently extruded through Millipore (Bedford, MA, USA) 0.1 μm pore-size polycarbonate filters using a LiposoFast extruder [147]. SUVs can be produced from the LUV by sonication using a probe sonicator or by extrusion through Millipore (Bedford, MA, USA) 0.03 μm pore-size polycarbonate filters using a LiposoFast extruder. The thickness of the bilayer in all vesicle types is 3-5 nm, depending on the length of the fatty acid chains [148, 149].

5. RESULTS AND DISCUSSION

The results and discussions presented below are mainly summaries of the corresponding papers, which are studies of applications of asymmetrical flow field-flow fractionation, supported by dynamic light scattering (DLS), size exclusion chromatography (SEC), and capillary electrochromatography (CEC). Using AsFlFFF, information such as particle sizes, molar masses, and the formation of aggregates can be obtained when the macromolecules or particles are made to change their physical or chemical characteristics by changes in factors like pH, ionic strength, temperature of the carrier solution, stoichiometric molar ratios of reactants and enzymatic treatment.

As discussed in chapter 2, in all the FFF-techniques the separation is achieved by applying a force field perpendicular to the transport direction [51]. Specifically, in FlFFF and its variant AsFlFFF, the field is a cross flow of carrier liquid perpendicular to the usual channel flow. The cross flow force pushes all particles toward the accumulation wall with the same velocity. The field strength is thus determined by the flow rate of this cross flow. Depending on the individual diffusion behavior of a particle, it will be relocalized, and eluted from the channel. Hence AsFlFFF separates particles based on their diffusion coefficients. From the retention data, it is possible to determine the diameter of the hydrodynamically equivalent sphere of the particle. The technique is suitable for aggregate formation studies as well, especially when the sample materials are exposed to changes in physico-chemical parameters such as pH, ionic strength, temperature, or to other factors like mechanical stress and biochemical interactions. In this thesis, the main emphasis was on AsFlFFF studies of particles or polymers, and on the use of this technique to study structural alterations of those particles. Both dynamic light scattering and size exclusion chromatography experiments were carried out, when necessary in parallel, to confirm the reliability of AsFlFFF results.

5.1. Effect of pH on protein/lipoprotein (I, V)

The structural stability and physical behavior of macromolecules with a hydroxyl group at the end or on a side chain are affected by the pH of the carrier solution. It is well known that

proteins quite easily aggregate at their isoelectric point with zero net charge due to the decreased electrostatic charge repulsion between the particles. At increased pH, the mass should disperse or disaggregate progressively as the net negative charge increases, whereas at decreased pH the mass should form colloids or aggregates as the net negative charge decreases. In this work, we studied the effect of pH on cytochrome c and low-density lipoprotein particles by AsFlFFF.

Cytochrome c (cyt c) is a small globular protein (104 amino acid residues, 12.4 kDa) carrying a large number of basic residues. Its pI value is about 10. Out of its 104 residues 24 are lysine, arginine and histidine, with pKa values of 10, 12 and 6.5, respectively. It is an electron-carrying mitochondrial protein as well as a heme protein, where the heme is covalently attached to cysteine amino acid residues. The ready alteration of cyt c between the ferrous and ferric states within the cell makes it an efficient biological electron-transporter. It plays a vital role in cellular oxidations in both plants and animals. It is generally regarded as a universal catalyst of respiration, forming an essential electron-bridge between the electron donors and acceptors. The protein serves as a very good model for studying the unfolding/refolding phenomena of the polypeptide chain with the heme participating simultaneously in the process without bimolecular recombination [150]. Naeem and Khan [151] showed the loss of approximately 61% and 65% helical secondary structure of cyt c at pH 9. Cytochrome c also has a single tryptophan residue at position 59, and Naeem and Khan observed an enhancement in tryptophan fluorescence at pH 9.0. The increase in the distance of the tryptophan from heme resulted in an increase in the fluorescence intensity and allowed detection of conformational changes occurring around the heme. The unfolding of cyt c increases the hydrodynamic particle diameter of the protein. In our study, the hydrodynamic particle diameter of cyt c was 4.1 nm at pH 11.4 and around 4.2 nm at pH 7.0 and 8.0. This increase in size at the two lower pH levels could be due to the partial unfolding of cyt c. In fact, a change in the size of cyt c probably is not the only cause of the observed effect, since interactions between the regenerated cellulose acetate ultrafiltration membrane (RP70PP) and the protein may also cause electrostatic repulsions, especially at higher pH, which shorten the retention times and decrease particle sizes. Lowering the pH may also lead to electrostatic attraction between the membrane and cyt c, which extends the retention time and increase the particle size.

With regard to lipoproteins, low-density lipoprotein (LDL) was chosen for pH studies. It is well recognized that LDL, has just one copy of apo-B protein, with a molar mass of 513 kDa, and the pI value ranges from pH 5.2 to pH 5.5. The carrier liquids used for fractionation of LDL samples were phosphate buffer at pH 7.4, 6.5, and 3.2, and acetate buffer at pH 5.0 and 4.0, with and without NaCl or EDTA concentrations. Our results show that, under the conditions employed, LDL particles remain intact. Thus, the sizes of LDL particles were similar (around 21-22 nm) at all pH levels tested. Even though apo B protein may change its conformation at different pH values or different ionic strengths (0-300 mM), it cannot be released from LDL and unfold unless some enzymatic reactions are involved such as proteolysis with α-chymotrypsin.

5.2. Effect of ionic strength (III)

The presence of background electrolyte (salt) in the carrier solution has been reported to affect the hydrodynamic volume and sizes of macromolecules and polymers in two ways [106, 108, 152]. Firstly, the effect is largely attributable to a diffuse double layer of charged ions. At very low ionic strength, the diffuse double layer extends some distance from the surface of the macromolecules, and the molecules become swollen and are expected to have an increased hydrodynamic size or volume. At higher ionic strengths, the diffuse double layer becomes thinner and the molecules become smaller in size but may collide with other molecules to form larger aggregated particles. The second effect of ionic strength variations on FlFFF can be attributed to exclusion volume effects, i.e., to the exclusion of sample molecules from near the accumulation wall. By this mechanism, component particles are forced away from the wall and into regions where the fluid velocity is higher. This effect also depends on the concentration of the sample injected into the FFF channel. At lower concentrations and lower ionic strengths, molecules having the same surface charge repel each other and are repelled from the accumulation wall of the channel (assuming the channel wall has the same sign charge), thus leading to shorter retention times and smaller particle sizes in AsFlFFF. The effect of ionic strength on retention in aqueous AsFlFFF is thus influenced by the electrostatic interactions among the macromolecules and the interaction between the macromolecules and the channel wall. Intramolecular electrostatic repulsion may also change the hydrodynamic size of the macromolecules in solution. This will eventually result in altered retention times in AsFlFFF. For this reason, DLS experiments were carried

out, when necessary, in parallel with AsFlFFF to verify ionic strength in the interaction between the macromolecules and the channel wall.

It is generally recognized that increased ionic strength in dispersions of electrostatically stabilized colloids shields the charges on the particle surface and decreases the thickness of the electrical double layer. This leads to increased attractive interactions between colloids, and due to collision of particles leads to the formation of aggregates or gel-like structures. The driving forces for the PEC formation are thus, coulomb interactions between oppositely charged polyelectrolytes plus the entropy gain when counterions are released. As a result, PECs are aggregated to form large particles. All PECs are very sensitive to changes in their environment, in particular to the addition of salts. For this reason our study (paper III) was mainly focused on the effect of ionic strength on polyelectrolytes, poly (methacryloxyethyl trimethylammonium chloride) (PMOTAC) and poly (ethylene oxide)-block-poly (sodium methacrylate), and on PECs (scheme 1).

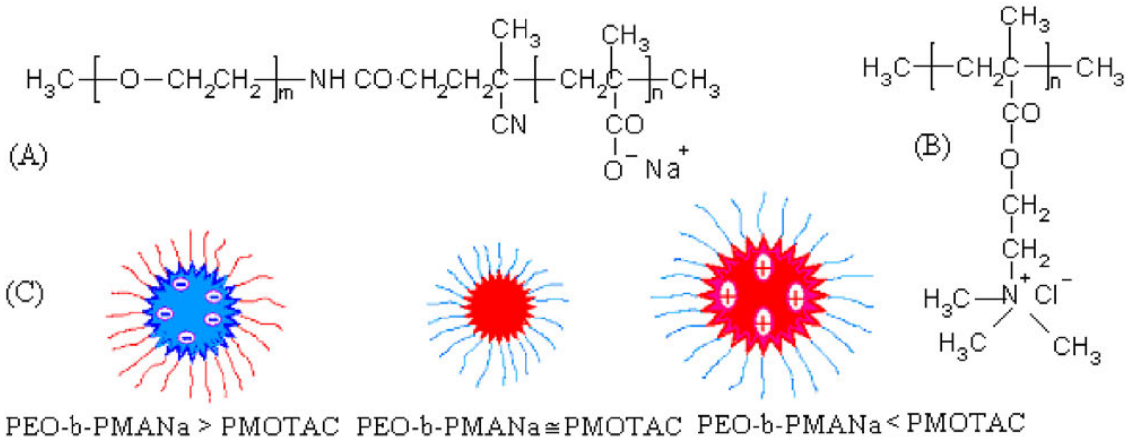

Scheme 1. *Schematic representation of PEO-b-PMANa (A), PMOTAC (B), and PEC (C).*

Polyelectrolyte complexes in solution using biological polymers were studied already in 1941 by Bundenberg de Jong [153], in 1965 by Michaels et al. [154], and in 1970 by Veis [155]. Polyelectrolyte complexes are formed mainly by strong electrostatic interactions between oppositely charged macromolecules, but hydrophobic interactions, van der Waals forces and hydrogen bonding can also play significant roles [156, 157]. The structure and composition of the PECs obtained depend on the degree of neutralization of the polyion, and on the polymer structure, hydrophobicity, concentration of the complex, pH and ionic strength [158]. In our study, the molar mass (Mw) of PMOTAC was 299 000 g mol^{-1}, as determined by SEC (0.8 M

aqueous $NaNO_3$ with 3 % acetonitrile as an eluent, calibration with poly (ethylene oxide) standards from 4 120 to 965 000 g/mol.). The molar mass (M_w) of PEO-b-PMANa was 22 800 g mol^{-1}, also as determined by SEC (Waters, 2410 RI-detector, Ultrahydrogel 250 and 2000 columns, 0.1 M aqueous $NaNO_3$ with 3 % acetonitrile as an eluent, using poly (acrylic acid) standards from 900 to 782 200 g/mol).

The effect of ionic strength of the cationic and anionic PEs in salt free solution or in the presence of 20, 80 and 160 mM NaCl was studied first. In salt free solution, the PEs were relatively larger in sizes than in the presence of NaCl solution (Table 2). As the ionic strength of the medium increased, the electrostatic repulsion between the polyelectrolyte monomer units decreased. At the same time, the polyelectrolyte chains become coiled, leading to the formation of more compact structures with relatively smaller particle sizes (scheme 1C**,** PEO-b-PMANa ≅ PMOTAC).

Table 2. *Diameters of PMOTAC and PEO-b-PMANa measured by AsFlFFF and DLS.*

NaCl/mM	PMOTAC				PEO-block-MANa			
	d_{peak} / nm		d_{mean} / nm		d_{peak} / nm		d_{mean} / nm	
	AsFlFFF	DLS	AsFlFFF	DLS	AsFlFFF	DLS	AsFlFFF	DLS
0	21.9	-	48.0	-	15.7	-	27.7	-
20	20.4	26.4	45.3	43.4	6.6	5.6	8.4	9.5
80	15.2	-	44.2	-	7.1	-	10.0	-
160	18.2	-	44.0	-	7.0	-	13.1	-

d_{peak} –diameter at peak.

d_{mean} –mean diameter.

In solution without salt, an interaction between the two oppositely charged polyelectrolyte polymers at an equivalent-mixing ratio of 1 was observed (Figure 11). Two peaks were seen in AsFlFFF fractogram (Figure 11a). The first peak was produced by the steric mode, and the second peak was produced by the normal mode, giving at peak a particle diameter of 130 nm and mean diameter of 134 nm. The steric mode results obtained in AsFlFFF were verified with independent DLS measurement, showing the presence of large aggregates with diameters of 2000 - 4000 nm, in addition to particles with a mean diameter of 157 nm (Figure 11b). In

this case the mean particle size in diameter obtained by AsFlFFF was 134 nm, where with DLS it was 157 nm.

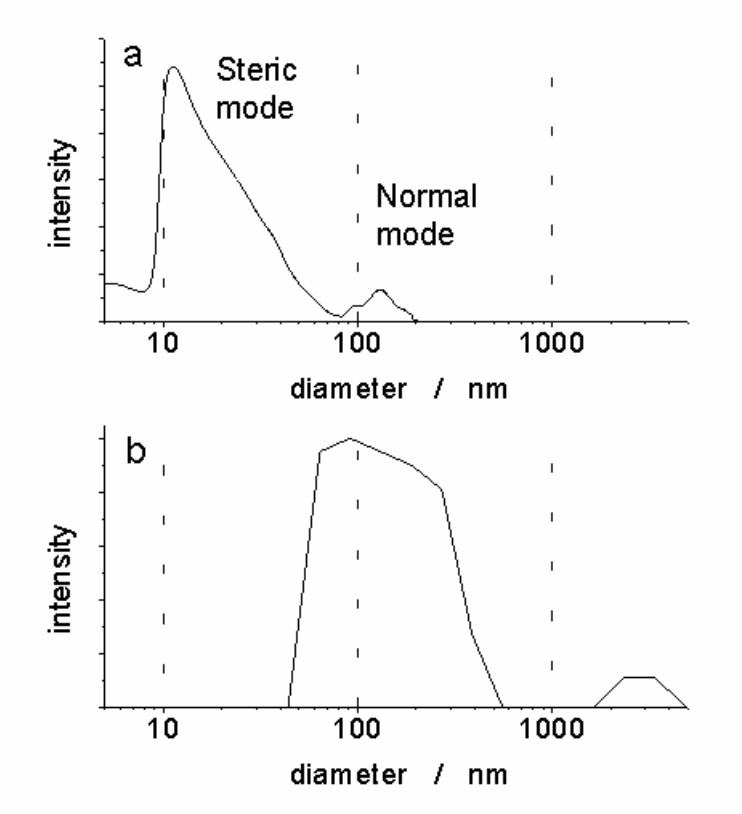

Figure 11. *Particle size distributions of PMOTAC/PEO-b-PMANa complexes at mixing ratio X=1 in salt-free solution. (a) AsFlFFF, first peak in steric mode, second peak in normal mode: d_{peak} 130 nm, d_{mean} 134 nm, (b) DLS, first d_{peak} 91 nm, d_{mean} 157 nm, second d_{peak} 3000 nm. Carrier liquid used in AsFlFFF was distilled water. Relaxation focusing: frontal flow rate 0.2 ml min^{-1}; flow inwards from outlet 2.6 ml min^{-1}; injection 1.0 ml min^{-1}for 5 minutes; relaxation time 30 minutes. Flow rates during elution period: $\dot{V}$ = 1.16 ml min^{-1}, $\dot{V}_c$ =1.0 ml min^{-1}; UV detection at 214 nm.*

In salt-free solution AsFlFFF easily determines the dimensions of the PEC; whereas in DLS various interactions due to the polyelectrolyte effect interfere with the scattering light could cause the particle size of the PEC. The effect of NaCl on PEC structures is described in section 5.5.1, together with the mixing ratio of PEs.

5.3. Influence of temperature on PNIPAM-temperature sensitive polymer (II)

A characteristic feature of certain aqueous polymer solutions is that phase separation can occur upon heating, due to their Lower Critical Solution Temperature (LCST). As used herein, the term "LCST" describes the temperature at which the polymer solution experiences a phase transition going from one phase (homogeneous solution) to a two-phase system (a polymer rich phase and a solvent rich phase) as the solution temperature increases. The LCST of aqueous solutions of polymers can easily be measured by optical density (referred to as cloud point) which appears as a point of inflection of the increase in absorbance that occurs upon raising the temperature [159]. However, in organic solvents, polymers usually display the opposite behavior, having an upper critical solution temperature (UCST), and meaning that they demix upon cooling [159]. Prominent examples of water-soluble polymers displaying inverse solubility upon heating (LCST) include poly (N-isopropylacrylamide)(PNIPAM) [160], methylhydroxypropyl cellulose (MHPC) [161], poly (vinylcaprolactam) (PVCa) [162], and hydrophobically modified ethyl hydroxyethyl cellulose [163]. Temperature sensitive PNIPAM polymer and its derivatives have attracted interest due to their potential use in many technological applications, including controlled drug delivery systems [164-166], the immobilization of enzymes [167], and capillary electrophoresis [168, 169]. PNIPAM is perhaps the most well known member of the class of temperature responsive polymers whose LCST in water is about 32 ^{o}C (Scheme 2). The exact temperature is a function of detailed microstructure of the polymer [160]. At temperatures lower than 32 ^{o}C, PNIPAM polymers are hydrated and form an expanded structure. Upon heating above the LCST the polymers dehydrate and change volume [170].

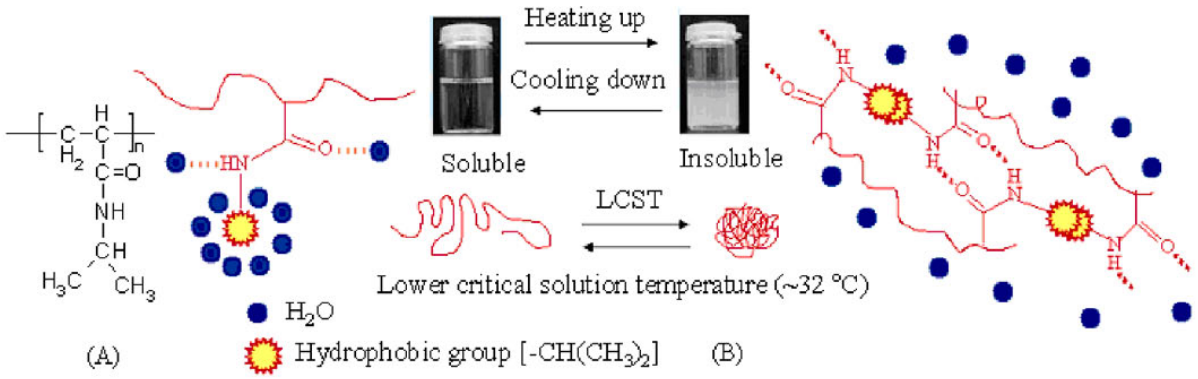

Scheme 2. *Schematic illustrations of poly (N-isopropylacrylamide (PNIPAM)) (A), Phase separation upon heating (B).*

In recent years considerable efforts have been made to characterize conformational changes of PNIPAM-based materials. Among other methods, DLS has been used to study the effect of temperature on the particle sizes of poly (N-isopropylacrylamide) (PNIPAM) homopolymers [171, 172], PNIPAM grafted with polymers such as polyethylene oxide [173], polyvinylpyrrolidone [174], polyacrylic acid and polymethacrylic acid [175].

The influence of temperature was examined with a PNIPAM homopolymer and a PNIPAM block copolymer with PEO, and both AsFlFFF and DLS techniques were used to monitor the effects. PNIPAM polymer particle sizes and molar masses were determined, and the results obtained with both techniques were compared with swollen, collapsed and aggregated polymers. The phase transition was also studied for polymers with different molecular architectures, including solutions of linear chain PNIPAM, and PNIPAM with PEO, employing AsFlFFF and DLS techniques.

In AsFlFFF, the hydrodynamic diameter, d_H as a function of the retention time is presented in Equation 20. In our PNIPAM study, the diffusion coefficient, retention time and hydrodynamic diameter were dependent on the applied temperature as well as on the viscosity of the carrier solution. The experimental temperatures were 25, 30, 32, 35, 37, 40, 45, and 50 ^{o}C; and their corresponding viscosities in millipascal second (mPa*s) were 0.8904, 0.7975, 0.7647, 0.7194, 0.6915, 0.6529, 0.596, and 0.5468, respectively.

The dependence of the average hydrodynamic diameters (d_H) on temperature obtained by AsFlFFF and DLS are shown in Figures 12A and 12B. At each experimental temperature, the time allowed for equilibration was 60 minutes for AsFlFFF and 30 minutes for DLS. The polymer amount loaded into the AsFlFFF channel was on average, 30 µg for PNIPAM_1, and 21 µg for PNIPAM-b-PEO. In DLS measurements, the concentration was 1.0 mg/ml, where the cuvette cell contained 1.5 ml, i.e. the measurement was done on 1500 µg of polymer in 1.5 ml of water solvent. The PNIPAM polymers underwent contraction and a volume phase transition when the LCST was approached. At the volume phase transition, polymer size was at its minimum. The average hydrodynamic diameters for the PNIPAM_1 polymers obtained by AsFlFFF were 17 nm at 25 ^{o}C, 15 nm at 30 ^{o}C, 12 nm at 32 ^{o}C, 13 nm at 35 ^{o}C, 26 nm at

37 ^{o}C, 32 nm at 40 ^{o}C, and 57 nm at 45 ^{o}C; and for PNIPAM-b-PEO polymers, 29 nm at 25 ^{o}C, 25 nm at 30 ^{o}C, 21 nm at 32 ^{o}C, 19 nm at 35 ^{o}C, 115 nm at 37 ^{o}C, 142 nm at 40 ^{o}C, 123 nm at 45 ^{o}C, and 121 at 50 ^{o}C (Figure 12A). The DLS results for PNIPAM_1 polymers were 19 nm at 25, 30, and 32 ^{o}C, 272 nm at 33 ^{o}C, 432 nm at 35 ^{o}C and 397 nm at 40 ^{o}C; and for PNIPAM-b-PEO polymers, 25 nm at 25 ^{o}C, 27 nm at 30 ^{o}C, 192 nm at 32 ^{o}C, 257 nm at 33 ^{o}C, 377 nm at 35 ^{o}C, and 380 nm at 40 ^{o}C (Figure 12B).

Based on the AsFlFFF results, the lower critical solution temperatures (LCST) for PNIPAM and PNIPAM-b-PEO were ~32 and ~35 ^{o}C, respectively (Figure 12A). The difference between the two polymer samples can be explained by the increased ability of PNIPAM to resist dehydration in the presence of PEO. Above the LCST, the polymer chains collapse upon heating. This collapse causes a decrease in the hydrogen bonding between water and PNIPAM molecules, which results in mutual attraction between polymer particles instead of repulsion. (Scheme 2B). Therefore, the particles formed larger aggregates as the temperature further exceeded the LCST.

The DLS results shown in Figure 12B reveal similar behavior as a function of temperature: from 25 ^{o}C to 32 ^{o}C, the particle size decreased slightly. However, above the critical solution temperature, the aggregated particle sizes as measured by DLS, abruptly increased. This is because in DLS, the collapsed PNIPAM aggregates are dependent on the concentration of the polymers. AsFlFFF gave less pronounced changes in particle sizes with temperature, and in the case of PNIPAM-b-PEO they were in agreement with the values reported by Virtanen and Tenhu, 2000 [176]. Furthermore, AsFlFFF provided roughly equal critical temperatures (ca 32 ^{o}C) as DLS for PNIPAM_1, but a 3^{o}C higher temperature for PNIPAM-b-PEO. The possible causes of the discrepancies in the aggregate particle sizes include concentration differences during thermal equilibration, and the fact that the AsFlFFF measurements were carried out under constant flow conditions, whereas in DLS the liquid was stationary. Moreover, in DLS the relative light scattered from the large particles obscures the light scattered from the smaller particles, hence the sensitivity is dependent on the particle size.

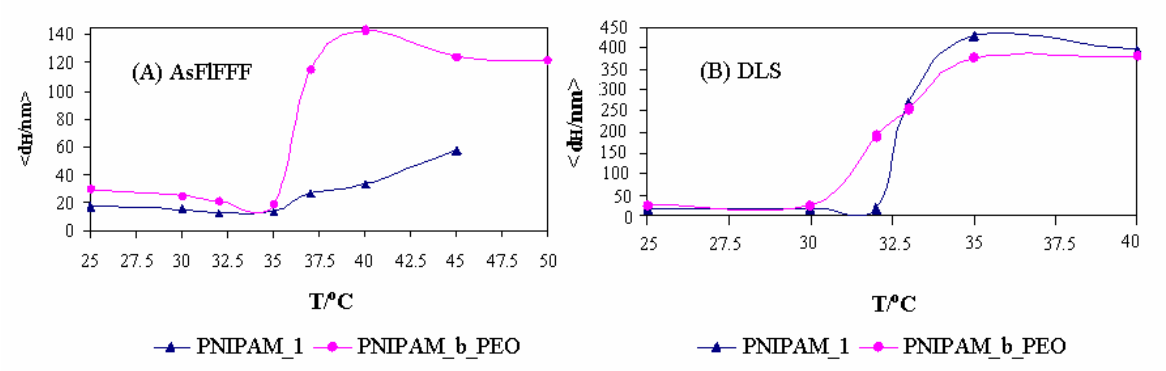

Figure 12. *Average hydrodynamic diameters (d_H) obtained by (A) AsFlFFF and (B) DLS for PNIPAM-b-PEO and PNIPAM-1 at various temperatures. AsFlFFF conditions are: Carrier-deionized water; relaxation focusing: flow rate at inlet 0.2 ml min^{-1}, flow inwards from outlet 2.6 ml min^{-1}; injection: 1.0 ml min^{-1} for 0.50 - 3.0 minutes; relaxation time 60 minutes. Flow rates during elution period: (A) $\dot{V}$ = 1.50 ml min^{-1}, $\dot{V}_c$ = 1.50 ml min^{-1}; (B) $\dot{V}$ = 1.75 ml min^{-1}, $\dot{V}_c$ = 1.25 ml min^{-1} at 25- 37 °C; $\dot{V}$ = 2.42 ml min^{-1}, $\dot{V}_c$ = 0.60 ml min^{-1} at 40-50 °C; UV detection at 210 nm.*

5.4. Influence of storage temperature on the stability of phospholipid vesicles (IV)

Upon dispersion in water, most of the phospholipids and mixtures spontaneously adopt bilayer structures above a certain critical micelle concentration (CMC) to form a closed vesicular structure. Such phospholipid dispersions, called liposomes, are frequently used as models for biological membranes, especially for delivering drugs to living cells [177]. Over the last decade, liposomes have been employed as vehicles to achieve specific delivery of drugs to target organs [178, 179]. For the many potential uses presented by liposomes, their application is dependent on the physical integrity and stability of the lipid bilayer structure. In fact, liposome instability is a major concern that prevents their application as industrially produced drug carriers. Good manufacturing processes must fabricate lipid vesicles that are as uniform in size as possible, and that remain stable for an acceptable shelf life at varying temperatures [180]. The most important quality of liposomes is that the chemical and physical stability of the vesicles in question should be maintained. Aggregation and fusion, which lead

to changes in particle sizes and particle size distributions, are the main results of the physical instability of phospholipid vesicles. Such processes occur to a significant extent over long periods of storage [181, 182]. Chemical stability involves prevention of both the hydrolysis of ester bonds in the phospholipid bilayer and the oxidation of unsaturated sites in the lipid chain. Chemical instability can lead to physical instability or leakage of an encapsulated drug from the bilayer, and fusion and aggregation of vesicles. Optical microscopy, cryo-electron microscopy, laser diffraction, and laser light scattering, among other techniques are commonly used for the determination of particle sizes of liposomes. The most straightforward method for measuring particle size is by quasi-elastic or dynamic light scattering that provides the mean diameter and polydispersity index of liposomes [183]. It can also distinguish whether the liposome population is uniformly distributed around one or more particle sizes (unimodal *versus* bimodal). In our study we used AsFlFFF and monitored whether physicochemical instability of liposomes was evident upon storage at +4 and –18 ^{o}C for an extended period of time. As a case study, egg yolk phosphatidylcholine (EPC) vesicles in the presence or absence of 20-mol% phosphatidylserine (PS) were used. Liposomes extrusion through a 100 nm polycarbonate filter was followed by measurement of the particle sizes by AsFlFFF, either immediately or after extrusion, or after storing them for several days or months. As seen in Figure 13, the EPC particle diameters at peak maximum and mean measured by AsFlFFF were 101± 3 nm and 122 ± 5 nm, respectively. No significant change in diameter was observed after storage at +4 ^{o}C for about five months. When the storage period was extended to about eight months (250 days) larger destabilized aggregates were formed (172 and 215 nm for peak maximum and mean diameters, respectively). Liposome size enlargement over time indicates aggregation due to physical and/or chemical instability. When EPC was stored at –18 ^{o}C, even only for one day, particles as large as 700 to 800 nm in diameter were formed as a result of dehydration, aggregation, and fusion processes. At low temperatures (-18 ^{o}C), the bilayer is extremely rigid and the perturbation produced by the interparticle contact will provoke changes in the orientation of the lipid molecules, facilitating disruption of the membrane.

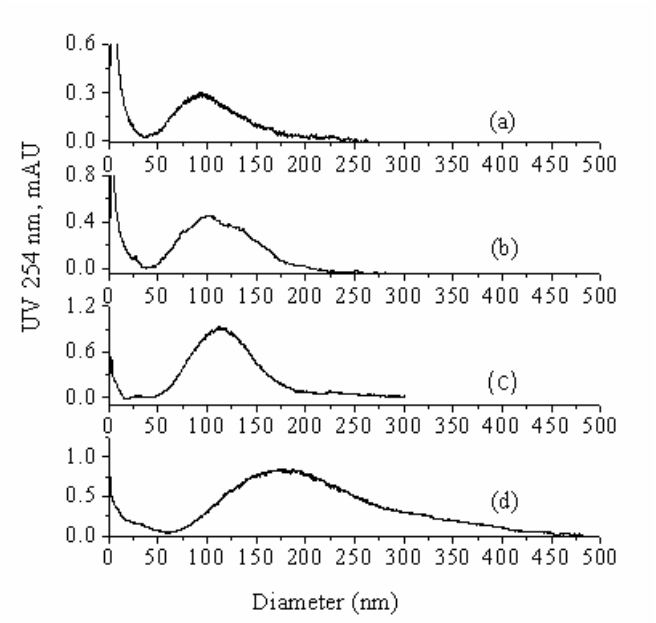

Figure 13. *Particle sizes of liposomes stored at +4 °C (a) for 14 days (EPC); (b) 164 days (EPC); (c) 164 days (80/20 mol% EPC/PS); and (d) 250 days (EPC). Experimental conditions: 8.5 mM phosphate buffer carrier, 0.02% NaN_3, pH 7.4; relaxation focusing: frontal flow rate 0.2 ml min^{-1}; flow inwards from outlet 2.6 ml min^{-1}; sample load 400 µl diluted to 20 ml, injection 1.0 ml min^{-1} for 10 min; relaxation time 30 min. Flow rates during elution period: $\dot{V}$ = 2.27 ml min^{-1}, $\dot{V}_c$ = 0.75 ml min^{-1}; UV detection at 254 nm.*

In the presence of calcium chloride, EPC alone did not form large aggregates, but the addition of 20-mol% of negatively charged phospholipids (PS, PA, PI, or PG) to the vesicles increased the electrostatic interactions between calcium ion and the vesicles and large aggregates were formed. Metal ions, such as calcium, make a bridge between two phospholipid molecules within one monolayer, or between molecules in two bilayers in contact with one another.

In the presence of cholesterol, large aggregates of about 250-350 nm appeared during storage at + 4 and –18 °C for more than one day. EPC vesicles, with or without 20-mol% PS, cholesterol or calcium chloride were used for coating of fused silica capillaries for electromigration studies. The electroosmotic flow (EOF) was suppressed due to the formation of phospholipid coatings (supported vesicle layer or supported lipid bilayer) and these were used for the separation of neutral model hydrophobic steroids. Liposomes stored at +25, +4, and −18 °C were studied at 25 °C and the performances of the coatings were evaluated by

measuring the EOF and the retention of steroids. Only minor differences were observed between the same phospholipid coatings, showing that phospholipid coatings in capillary electromigration techniques are relatively insensitive to storage at +25, +4 °C or −18 °C.

5.5. Influence of reactants on the formation of aggregated particles (I, III, V)

In sections 5.1-5.4, the effects of pH, ionic strength, and temperature of the carrier solution on the formation of aggregates were described. In this chapter, the discussion is mainly focused on the effect of reactants on the formation of aggregated particles. The mixing molar ratios of protein and lipid, polyelectrolyte solutions and enzymatic and biochemical effects on aggregation and fusion of low-density lipoproteins were studied.

5.5.1. Complex formation between protein and lipid (I)

The interaction of cyt c with liposomes has been considered as a model for interactions between peripheral proteins and membrane lipids. The nature of cyt c-acidic lipid interactions is strongly influenced by the charge density and mixing molar ratio of the interacting lipid surface to cyt c, as well as by the ionic strength and pH of the medium [184 - 186]. Several studies have reported that cyt c binding to a lipid bilayer involves numerous types of interactions. Among others, these interactions can include formation of electrostatic contacts as well as hydrogen bonding between the amino acid side chains and phospholipid head groups, and hydrophobic protein-lipid interactions originating from the penetration of the non-polar amino acid residues into the membrane hydrocarbon region (i.e. incorporation of the lipid acyl chain into the hydrophobic cavity of the protein molecule) [186 - 188]. Both electrostatic and hydrophobic interactions have been found to be the most important factors in the interaction between cyt c and liposomes. Studies conducted with model systems have indicated that two different cyt c sites, referred to as the A and C sites, are responsible for the association with lipid bilayers [189, 190]. Binding to site A is considered to involve electrostatic interactions between the phosphate head group of the bilayer and basic amino acid residues such as lysine, and arginine. Site C contains hydrophobic residues that accommodate one phospholipid acyl chain [189, 190].

The aim of our study was to investigate the aggregation of cyt c, and to distinguish between the hydrophobic and electrostatic interactions between the protein and lipid as the pH of the medium and DMPG (liposome) cyt c mixing molar ratio vary. Cyt c was prepared 15 µM, at pHs 7.0, 8.0 and 11.4, and an aliquot was taken and diluted to a final concentration of 0.25-1.5 µM. The stock solution of DMPG was 1 mM which was diluted to 1.5 or 15 µM. Experiments were carried out at 0-180 DMPG/cyt c molar mixing ratios. The heme group of cyt c absorbs visible light at ~410 nm wavelength, where as DMPG is transparent. As a result, the visible light detector at 410 nm due to the presence of cyt c was used. At a DMPG/cyt c molar mixing ratio of 10, at pH 7.0, 8.0, and 11.4, the particle diameters at peak maximum were 18.0, 12.9, and 5.6 nm, respectively (Figure 14). At pH 7.0 or 8.0, cyt c is obviously positively charged and DMPG is negatively charged. At these pH levels, the positively charged amino acids of cyt c, lysine and arginine respectively, mediate the ionic interaction with the negatively charged phosphate head group of DMPG.

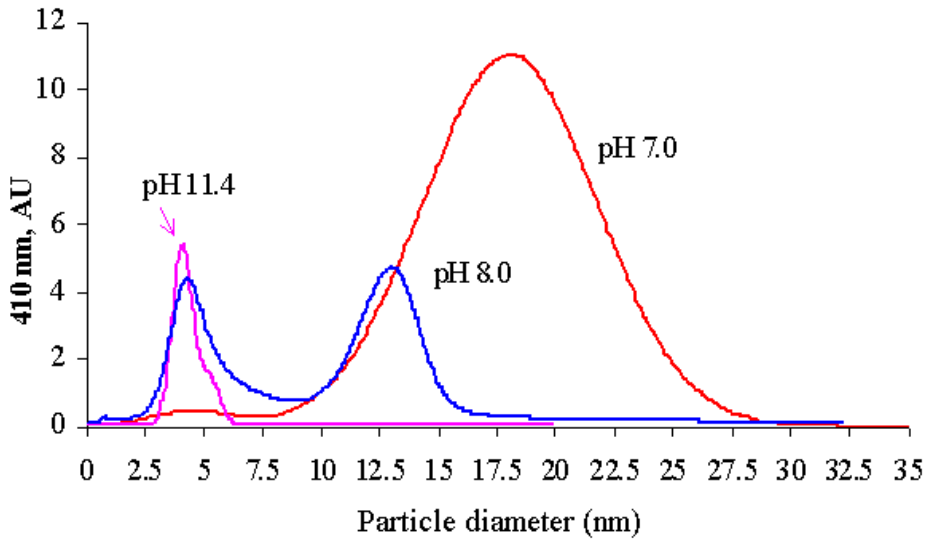

Figure 14. *Particle diameters obtained for DMPG/cyt c at a molar ratio of 10, at pH 7.0, 8.0, and 11.4. Carrier in AsFlFFF: 5 mM phosphate buffer, 0.02% NaN_3, pH 11.4; relaxation focusing: frontal flow rate of 0.2 ml min^{-1}, flow inwards from outlet at 2.6 ml min^{-1}; injection: 1.0 ml min^{-1} for 2-3 minutes; relaxation time 30 min. Flow rates during elution period: $\dot{V}$ = 0.6 ml min^{-1} , $\dot{V}_c$ = 2.44 ml min^{-1}; UV detection at 410 nm.*

In contrast, at pH 11.4 cyt c is negatively charged so there is no electrostatic attraction, and so hydrophobic interactions between the hydrophobic part of cyt c and DMPG become significant. As a result, the structure of cyt c is altered and DMPG is bound to cyt c at pH 11.4; only with a DMPG/cyt c molar ratio ≥10 (Figure 15), as evidenced by the occurrence of two peaks. The first peak is similar to native cyt c whereas the second peak, with an average diameter of 5.5 nm at peak maximum, is probably due to complex formation between cyt c and monomer DMPG. In the particle with a diameter of 5.5 nm, cyt c could be in the so-called molten globule (MG) conformation with bound DMPG. This compact and flexible state has been suggested to be associated with the binding and insertion of proteins into lipid bilayers [191 - 194]. The secondary structure of the MG state remains the same as in the native protein, whereas the tertiary structure is disrupted, and the overall structure becomes looser.

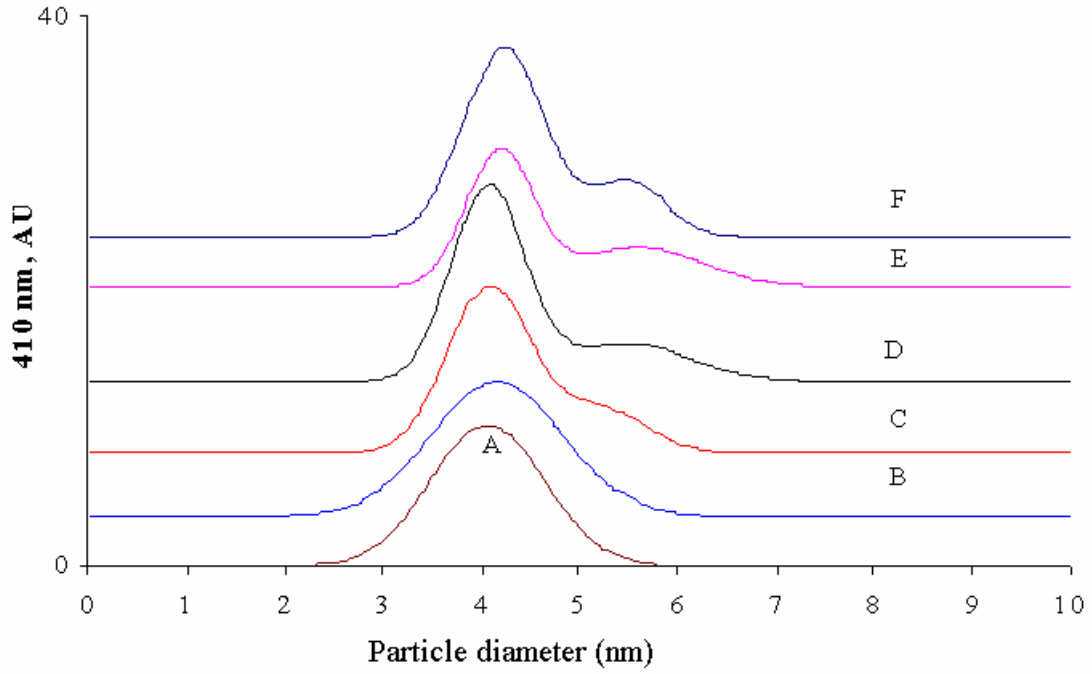

Figure 15. *Particle diameters of DMPG/cyt c complexes at pH 11.4. The DMPG/cyt c molar ratios were: (A) 0, (B) 1, (C) 10, (D) 20, (E) 30, and (F) 60. AsFlFFF operational conditions were the same as in Figure 16.*

To investigate analogous binding of cyt c with lipid, the DMPG was replaced with oleic acid and similar particle diameters were obtained as for DMPG/cyt c at pH 7.0 and 8.0. We also investigated binding of the anionic detergent SDS with cyt c. Particle diameters remained approximately 4.2 nm both in the absence and presence of SDS and did not change

significantly at pH 7.0 or pH 8.0. However, a second peak with a diameter in the range of 5.4 to 7.3 nm emerged when the SDS/cyt c molar ratio exceeded 260. In an earlier study, Yoshimoto *et al.*, 1999, investigated the interactions between cyt c and phosphatidylcholine by using gel permeation chromatography with immobilized phospholipid vesicles [195]. In agreement with our results, these authors reported two states for cyt c; the native conformation, and a conformation bound to the vesicle. Kinnunen and coworkers have also previously suggested two distinct acidic phospholipid-binding sites (A and C) in cyt c [189, 190].

5.5.2. Polyelectrolyte mixing ratio (III)

In the PEC study, both the stoichiometric and nonstoichiometric mixing molar ratios along with ionic strength were considered. Stoichiometric complexes are formed between the polyions at a 1:1 mixing ratio. Non-stoichiometric complexes consist of a charge neutralized core, surrounded by an electrostatically stabilizing shell composed of the excess overcharged component. Salt also has a significant effect on the formation of PECs, because it weakens electrostatic interactions, strengthens screening effects, and enables rearrangement processes [196]. Thus, the presence of a small amount of NaCl salt results in formation of smaller particles. The increase in ionic strength in such a system leads to secondary aggregation and the formation of bigger particles [196 - 199].

Figure 16 shows the dependence of PEC particle size on the mixing ratio and the ionic strength of the medium, as examined by AsFlFFF. As the ionic strength of the solution increases from 20 to 80 and 160 mM NaCl, the complexes get looser due to secondary aggregate formation, and the particle size increases. At the stoichiometric ratio of X=1 (Scheme 1c), particles with a hydrophobic core and a hydrophilic shell have the most compact structure [200]. As the amount of anionic PEO-b-PMANa, increases (i.e. the mixing ratio X=[MOTAC]/[PMANa] decreases), the mean diameter of the main peak first increases and then decreases, and finally the concentrations of the particles are too low to be detected by the AsFlFFF technique. The higher the degree of overcharging of the PEC particles, the looser the structure of the particles becomes, until finally the PEC particles disintegrate.

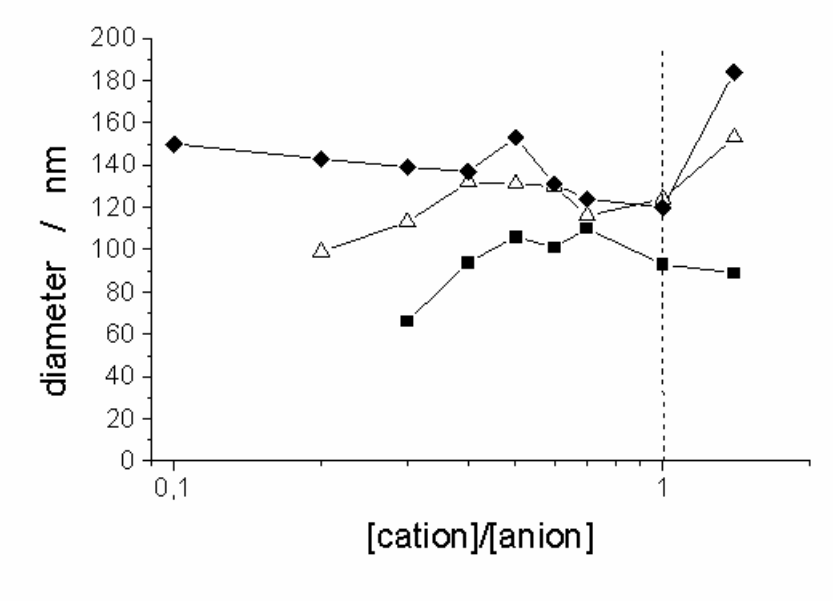

Figure 16. *Particle sizes obtained by AsFlFFF at various PMOTAC/PEO-b-PMANa mixing ratios, X (X=[cation][/anion]) in 20 mM (■), 80 mM (△), and 160 mM (♦) NaCl solutions.*

The PEC particle size distributions at various ionic strengths and molar mixing ratio X (X=MOTAC]/[PMANa]) are clearly seen in Figure 17. At the lowest ionic strength, 20 mM (Figure 17a), the particle size distributions, at X=0.7-1.0, showed monodispersed PECs. At the others mixing ratios, X=0.3-0.5 and X =1.4, there was excess charged polyelectrolyte. This caused splitting of the particles, leading to PECs in different equilibrium states. At a mixing ratio of 0.2, the PEC particles were below the detection limit of AsFlFFF but they were still observed by DLS (Table 3).

At ionic strengths 80 and 160 mM (Figures 16, 17b and 17c), PECs were observed at mixing ratios as low as 0.2 and 0.1, respectively. At mixing ratios of 0.1 and 0.05, respectively, the number of PECs was below the detection limit of AsFlFFF. At mixing ratios of 0.1 and 0.05, respectively, PEC particles were below the detection limit of AsFlFFF, but they were still observed by DLS (see Table 3).

At an ionic strength 80 mM, the reason for the bimodality of the particle sizes distribution of the X=1 particles is not clear. According to DLS, the size distribution of stoichiometric PECs was also bimodal but the minor component arose from the secondary aggregation of PECs [200]. The average particle sizes of the PECs obtained by both AsFlFFF and DLS, calculated

as weighted averages of the size distributions, coincide perfectly. This verifies that polymer repulsion from the accumulation wall did not affect the results obtained by AsFlFFF.

Table 3. *Particle sizes of PMOTAC/PEO-block-PMANa PECs at ionic strengths of 20 mM and 80 mM NaCl measured by AsFlFFF and DLS.*

Cation/anion	Diameters of PECs in 20 mM NaCl				Diameters of PECs in 80 mM NaCl			
	d_{peak} / nm		d_{mean} / nm		d_{peak} / nm		d_{mean} / nm	
	AsFlFFF	DLS [200]	AsFlFFF	DLS [200]	AsFlFFF	DLS [200]	AsFlFFF	DLS [200]
3.3	0[a]	35	0[a]	40	0[a]	166	0[a]	162
1.4	68	76	89	72	116	115	153	124
1.0	88	85	93	71	111	109	124	99/202[b]
0.7	96	74	110	110	106	126	116	127
0.6	90	-[a]	101	-[a]	115	-[a]	130	-[a]
0.5	89	-[a]	106	-[a]	113	-[a]	131	-[a]
0.4	86	-[a]	94	-[a]	105	-[a]	132	-[a]
0.3	64	66	66	67	94	92	113	138
0.2	0	42	0	61	90	113	99	125
0.1	-[a]	55	-[a]	69	0[a]	118	0[a]	118

d_{peak} – the peak value of the size distribution.

d_{mean} – mean diameter of the size distribution.

[a] 0 stands for below detection limit and - for not determined.

b Bimodal distribution; the mean diameter of the main peak is 99 nm and the averaged of the two peaks is 202 nm [200].

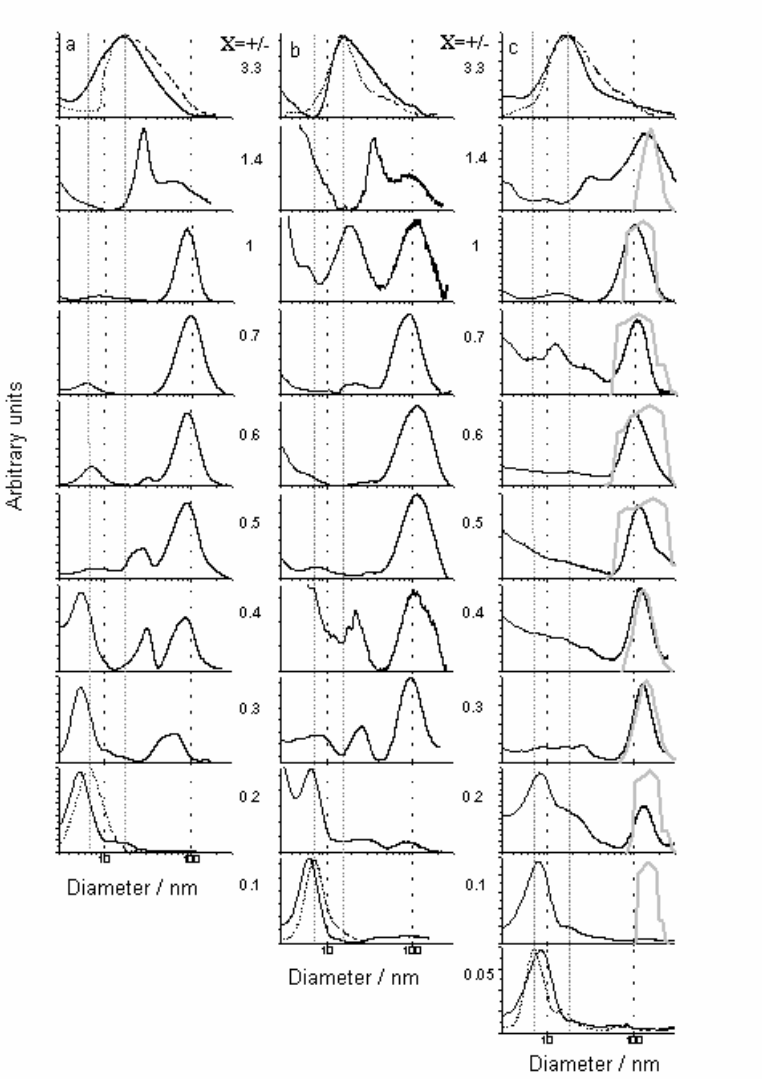

Figure 17. *Particle sizes of polyelectrolyte complexes measured by AsFlFFF (solid lines), and DLS (gray lines) at various mixing ratios X, at ionic strengths of (a) 20 mM NaCl, (b) 80 mM NaCl, and (c) 160 mM NaCl. The size distributions of pure PMOTAC and PEO-b-PMANa measured by AsFlFFF are shown as dotted lines. Relaxation focusing: frontal flow rate 0.2 ml min^{-1}, flow inwards from outlet 2.6 ml min^{-1}; injection at 1.0 ml min^{-1} for 3–7 min; relaxation time 30 min. Flow rates during elution period: $\dot{V}$ = 0.2 ml min^{-1}, $\dot{V}_c$ =2.9 ml min^{-1}, for PEO-b-PMANa; $\dot{V}$ = 0.8 ml min^{-1}, $\dot{V}_c$ =2.3 ml min^{-1}, for PMOTAC; $\dot{V}$ = 1.2-1.4 ml min^{-1}, $\dot{V}_c$ =1.7-1.9 ml min^{-1} for PEC; UV detection at 214 nm.(DLS results using 20 and 80 mM NaCl are in ref. 200).*

5.5.3. Effect of enzymatic and chemical treatments on aggregation and fusion of LDL (V)

Plasma lipoproteins can be divided into five major subclasses on the basis of the density at which they float during ultracentrifugation. Lipoprotein subclasses are further divided according to particle size, electrical charge and apolipoprotein and lipid contents. Table 4 outlines the most important features of the major lipoprotein species, namely chylomicrons, very low-density lipoprotein (VLDL), intermediate density lipoprotein (IDL), low-density lipoprotein (LDL) and high-density lipoproteins (HDL2 and HDL3).

In our case study, the average hydrodynamic diameter obtained using mAsFlFFF for HDL3, HDL2, LDL, and VLDL at pH 7.4 (8.5 mM phosphate buffer containing 1 mM EDTA and 150 mM NaCl) were 8.6 ±0.5, 11.2± 0.2, 22.1± 0.7, and 48.9±7.5 nm, respectively. Our results were all within the range of the literature cited values in Table 4.

Table 4. *Classification of lipoproteins (source data from Schultz and Liebman, 2002) [201].*

Classes	Diameter nm	Density g/mol	Apolipoproteins	Composition (mass %)				
				Protein	Lipids			
					TG	PL	CE	PC
Chylomicrons	75-1200	<0.95	AI,II,IV;B-48; I,II;III;E	1-2	88	8	3	1
VLDL	30-80	0.96-1.006	B-100;CI,II;III;E	11	54	15	14	6
IDL	25-35	1.006-1.019	B-100;CI,II;III;E	18	31	22	23	6
LDL	18-25	1.019-.0631	B-100	25	3	21	42	9
HDL2	9-13	1.063-1.25	AI,II,IV;CI,II,III;D:E	43	2	30	20	5
HDL3	7-9	1.125-.1.21	AI,II,IV;CI,II,III;D	55	1	25	16	3

The particle size of LDL is one of major factors causing formation of foamy cells. LDL aggregation and retention have been reported to be the initial steps in the development of atherosclerosis as described by Williams and Tabas in 1995 and 1998, as a result of the response-to-retention hypothesis [202, 203]. During the initiation of atherosclerosis,

cholesterol derived from LDL particles accumulates in the intima, which is the inner layer of the arterial wall [204]. These retained particles appear foamy, like the macrophages that result from the accumulation of cholesterol esters from LDL and lead to plaque formation [205]. The native LDL particle, with an average size of 22 nm, easily diffuses through the intima layer. However, if the particle size becomes larger than the native particle size, the particles would be trapped in the intima. There are many factors known to facilitate LDL aggregation and fusion such as enzymatic apoB proteolysis [206] and enzymatic lipid hydrolysis [205], and oxidation [207].

Variations in concentration, composition, and particle sizes of low-density lipoprotein are factors in the development of atherosclerosis, the leading cause of heart failure. In our case study, the aim was to investigate aggregation or fusion of LDL particles by AsFlFFF when LDL particles were modified *in vitro* by proteolytic and lipolytic enzymes, as well as by mechanical disruption and a chemical oxidizing agent.

Figure 18 shows the fractograms obtained at 22 ºC and pH 7.4 for native LDL and for LDL treated with the neutral proteases α-CT, PLA2, and Smase. α-CT-treated LDL and SMase-treated LDL showed a peak at 20–22 nm corresponding to the size of native LDL particles. In addition, α-CT-treated LDL showed a peak at about 30 nm, indicating the formation of larger particles, and a peak at 5 nm, indicating a release of peptide fragments from LDL particles. In the case of SMase, in addition to the 20-22 nm peak, there was a second large peak having a mean hydrodynamic diameter of 55 nm. Öörni et al. [208], recently reported that LDL particles become only slightly aggregated with α-CT but strongly aggregated when treated with SMase. Accordingly, it is likely that the larger particles seen in Figure 18 are fused in the α-CT-treated LDL sample and aggregated/fused in the SMase-treated LDL sample. PLA2-treated LDL showed particle sizes of 24-25 nm as a result of aggregation. SMase is known to be present in the arteries, *in vivo*, due to its secretion from endothelial cells of the arterial wall [205, 209, 210]. SMase is reported to accelerate the aggregation of LDL through its cleavage of the phosphocholine group of sphingomyelin, resulting in the generation of the hydrophobic moiety ceramide [210].

LDL aggregates prepared *in vitro* by vortex mixing and oxidation with copper has also shown macrophage-derived foam cell formations. Conventional AsFlFFF showed particles derived from brief vortexing with average 500 nm hydrodynamic diameter and a range of 300 nm to 700 nm, in agreement with reports by Khoo et al. [211] and Guyton et al. [212]. Oxidation with copper sulfate gave (average particle size) of about 100 nm.

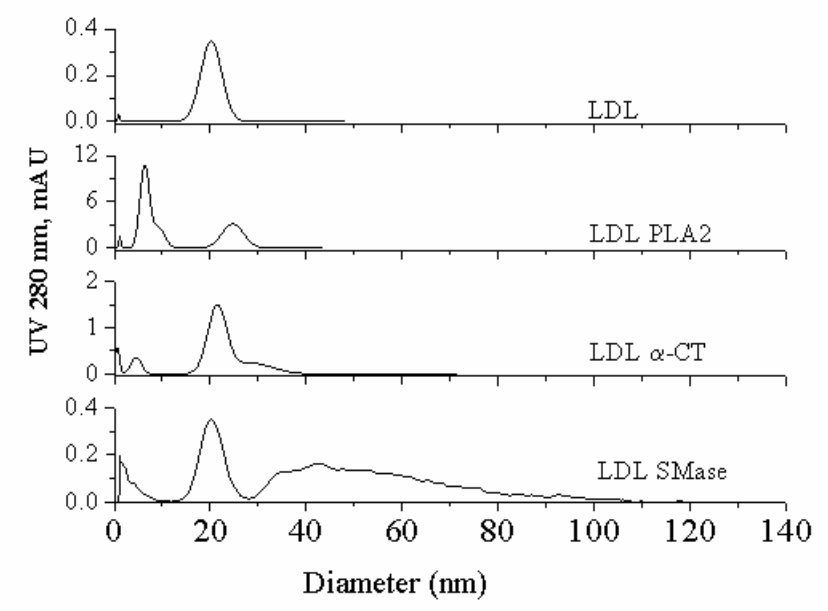

Figure 18. *Effects of PLA2, α-CT and SMase on LDL particle sizes as measured by mAsFlFFF. Carrier: 8.5 mM phosphate buffer (pH 7.4), 0.02% NaN_3, 150 mM NaCl; Ionic strength (IS) due to buffer, 20 mM. Relaxation focusing flow rate at inlet 0.1 ml min^{-1}; flow inward from outlet 1.4 ml min^{-1}; injection 0.5 ml $min^{-1}$for 1–2 min; relaxation time 20 min. Flow rates during elution period: $\dot{V}$ = 0.30 ml min^{-1}, $\dot{V}_c$ = 0.52 ml min^{-1}; UV detection at 280 nm.*

5.6. Conversion of diffusion coefficient to molar mass determination (I, II)

Retention time (in AsFlFFF) depends on the diffusion coefficient. In our case study, we used AsFlFFF to determine the molar masses of the cyt c-DMPG complex and PNIPAM polymers. First, the diffusion coefficients of protein standards, PSS and PEO respectively were obtained. Then the logarithms of diffusion coefficients (D) were plotted (Figure 19) against the logarithms of the molar masses through the empirical equation [213]:

$$D = AM^{-b} \quad (36)$$

where A and *b* are empirically determined constants for a given polymer-solvent-temperature system. The log/log model can be expressed as:

$$\log(D) = \log(A) - b(\log(M)) \quad (37)$$

Log (A) is an intercept and –b is a slope of the plot. The absolute value of b is a scaling factor, related to the shape of the chain and provides information about the polymer-solvent interactions and macromolecular conformation of the polymer.

The carrier medium used for the separation of proteins and polystyrene sulphonate standards was 5 mM phosphate buffer at pH 7.0. The ionic strength due to the buffer was 8.8 mM. Deionized water at neutral pH was used for the fractionation of PNIPAM and PEO polymers. The experimental molar masses for the protein standards were 12.4, 25, 66.43, 250, 440, and 669 kDa for cyt c, chymotrypsinogen A, BSA, catalase, ferritin and thyroglobulin respectively, and their corresponding diffusion coefficients at peak, in $cm^2\ s^{-1}$ x 10^{-7} were 10.9, 8.1, 6.2, 3.5, 2.9, and 2.1 respectively. The molar masses for PSS in g mol^{-1} were 6780, 7640, 13200, 320000, 57500, 126700, and 262600, and their corresponding diffusion coefficients at peak, in $cm^2\ s^{-1}$ x 10^{-7} were 11.55, 10.77, 7.81, 4.67, 3.54, 2.06, and 1.39 respectively. The molar masses for PEO in g mol^{-1} were 7500, 20300, 29600, 58400, 74900 and 124700; and their corresponding diffusion coefficients at peak, in $cm^2\ s^{-1}$ x 10^{-7} were 5.86, 4.64, 3.82, 2.23, 1.50, and 0.98 respectively.

The plot of logarithm of the diffusion coefficient versus logarithm of molar mass for proteins, PSS, and PEO is presented in Figure 19 based on Equation 37. For compact spheres, the theoretical value for b is 0.33; for random coils in theta solvents and in good solvents it is 0.5 and 0.6 respectively; and for rigid rod-like polymers it is 1.0 [214]. It can be noted here that proteins are hydrated particles in aqueous buffers and cannot generally be taken to be hard spheres. From the plot, values of 0.39 for the globular proteins, 0.58 for PSS and 0.66 for PEO were found. The scaling factor for proteins obtained in this study was very close to the value of 0.38 reported by Litzén [215] and 0.38±0.04 reported by Wijnhoven *et al*. [152]. The molar mass of 12.3 kDa for cyt c obtained from the calibration curve is in agreement with the nominal value of 12.4 kDa. The DMPG/cyt c complex is assumed to adopt a flexible random

coil polymer conformation in aqueous solutions because of the unfolding of cyt c. Therefore, the relationship between diffusion coefficient and globular protein structure does not directly apply for the molar mass of cyt c/ DMPG complex.

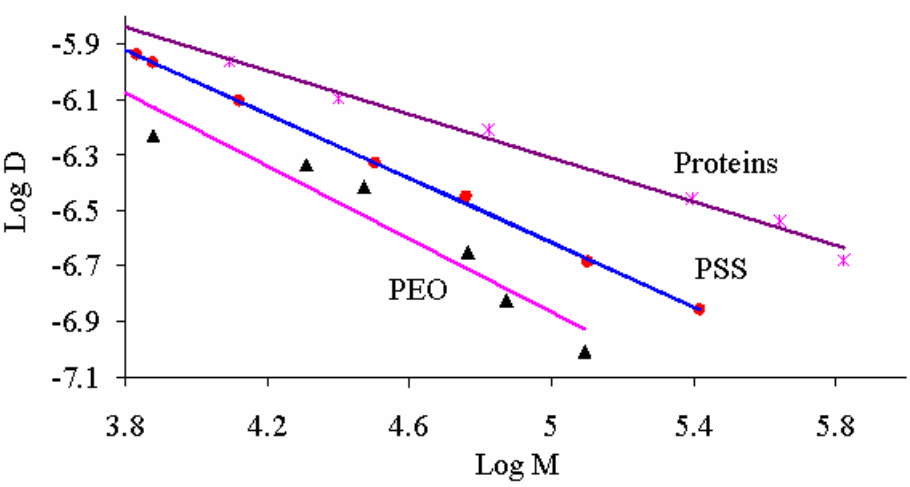

Figure 19. *Plots of the logarithm of the diffusion coefficient D (cm^2/s) versus the logarithm of the molar mass (M) obtained from the fractograms of proteins, PSS, and PEO standards.*

The calibration plot made from the protein standards did not allow of the conversion of PNIPAM polymer diffusion coefficient to molar masses due to differences in macromolecular conformational structure, and the less favorable protein-hydration properties than in case of PSS or PEO polymer-water interactions. Since most of the PNIPAM samples were non-ionic, the universal constants obtained from PEO were used for the PNIPAM polymer molar mass calculations. The molar masses of PNIPAM polymers were then calculated using equation 37 and compared to the molar masses obtained by SEC (Table 5). The two methods gave quite similar molar masses and polydispersity indices, even though the peak shapes obtained by AsFlFFF and SEC looked different. In SEC, particles with a larger mass eluted prior to those with a smaller mass, whether retention was measured in terms of time or volume. In contrast, for AsF1FFF the situation was reversed, with smaller mass particles eluting before larger mass particles. However, a better molar mass was obtained for PNIPAM for which a molar mass of 160 kDa which was obtained by static light scattering. The molar mass given by SEC was only 33 kDa, compared to 175 kDa given by AsFlFFF (Figure 20). It can be noted here that AsFlFFF can provide a good estimation for molar masses under certain circumstances. The main advantage of AsFlFFF over SEC can be attributed to the absence of porous column packing materials [216, 217]. The open channel in AsFlFFF reduces the opportunity for

sample membrane adsorption. Another advantage of AsFlFFF is the flow through the open channel is laminar and less tortuous than in the packed column of SEC. For large aggregate analysis, SEC starts to become ineffective, because shear force can degrade the analytes; there is no such problem with AsFlFFF.

Table 5. *PNIPAM molar masses and PDI measured by AsFlFFF and SEC.*

Polymer sample	AsFlFFF			SEC		
	Mn	Mw	PDI	Mn	Mw	PDI
PNIPAM_1	28200	35900	1.27	19900	39500	1.98
PNIPAM_2	13600	17500	1.29	10900	16600	1.52
PNIPAM_3	8650	13000	1.39	9500	16200	1.71
PNIPAM-b-PEO	56400	102400	1.80	43000	83000	1.94
PNIPAM-M-160 kDa	105700	174800	1.65	23900	33000	1.38
PNIPAM-cpa-RAFT-1	5630	6900	1.22	5830	6390	1.10
PNIPAM-cpa-RAFT-2	7850	9100	1.16	9280	10100	1.09
PNIPAM-cpa-RAFT-3	4650	4990	1.07	2620	3090	1.18
PNIPAM-cpa-RAFT-4	8550	10400	1.21	9100	10900	1.12
PNIPAM-cpa-RAFT-5	5730	6270	1.09	5400	6100	1.13
PNIPAM-cpa-RAFT-6	10000	15300	1.52	11900	14200	1.19

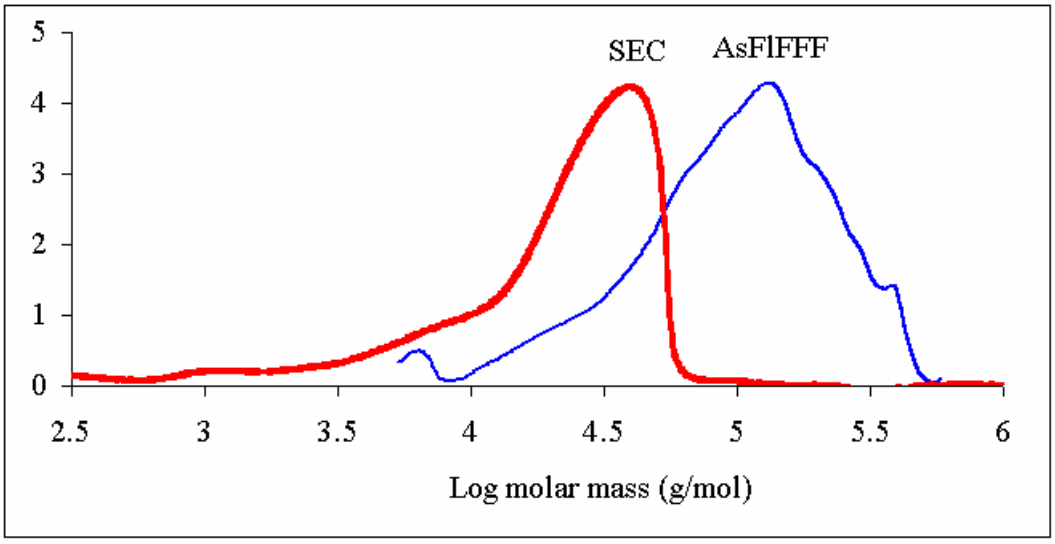

Figure 20. *Molar mass distributions of PNIPAM (M=160 kDa) determined by AsFlFFF and SEC.*

6. CONCLUSIONS

In this work asymmetrical flow field-flow fractionation (AsFlFFF) was used for macromolecule chemistry studies. The effects of several parameters, such as temperature, pH, ionic strength, and the reactant mixing ratios on the particle sizes, molar masses, and the formation of aggregates of macromolecules were clarified.

The effect of temperature was studied in the characterization of the hydrodynamic particle sizes, molar masses, and polydispersity of various thermo-responsive poly (N-isopropylacrylamide) (PNIPAM) polymers. At ambient temperature (~25 ^{o}C), the polymers were swollen and well hydrated, and when the temperature exceeded about 30 ^{o}C, the polymers started to shrink, resulting in smaller size. The minimum particle sizes were seen at ~32 ^{o}C. At 35 ^{o}C and above, water molecules were repulsed, so that hydrophobic interaction predominated, leading to formation of aggregates. When the linear PNIPAM polymer was replaced with PNIPAM-b-PEO, the minimum particle sizes were seen at temperatures ~35 ^{o}C, due to the hydrophilic nature of the PEO polymer, which increased the ability of the PNIPAM component to resist dehydration. The molar mass analyses of PNIPAM polymers were made at a fixed temperature (25 ^{o}C). The polymers were synthesized either via free radical polymerization or via reversible addition-fragmentation chain transfer (RAFT). The polydispersity index in the first case was relatively high (about 2) indicating that free radical polymerization is not easily controllable, in contrast to polymerization via RAFT (polydispersity index ~1).

The pH of the solution played an important role when the interactions between cyt c and an acidic phospholipid DMPG, were investigated at different mixing molar ratios. At pH 11.4, with a DMPG/cyt c mixing molar ratio ≥10, the AsFlFFF elution profile showed two peaks. The first peak was similar to native cyt c with average diameter of 4 nm, whereas the second peak, with an average diameter of 5.5 nm, was probably caused by complex formation between cyt c and monomer DMPG. Because at pH 11.4 both cyt c and DMPG bear negative charges, the electrostatic interactions between cyt c and DMPG were negligible. However, hydrophobic interactions between the hydrophobic part of cyt c and DMPG were possible. At pH values 7.0 and 8.0, the structure of cyt c was probably altered, and DMPG was bound to

cyt c with net positive charges. At these pH values, with a DMPG/cyt c mixing molar ratio ≥ 10, the AsFlFFF elution profile showed two peaks. The first peak was similar to native cyt c with an average diameter of 4 nm, whereas the second peak gave average diameters of 18 and 13 nm at pH 7.0 and 8.0 respectively, mainly due to major electrostatic and minor hydrophobic interactions. By replacing the lipid DMPG with oleic acid, electrostatic interactions at pH 7.0 and 8.0 exhibited, but when replaced with SDS, only hydrophobic interactions were seen.

At neutral pH, the effects of salt and molar ratios of polycations and polyanions on the hydrodynamic diameters of cationic poly (methacryloyloxyethyl trimethylammonium chloride), PMOTAC, and anionic poly (ethylene oxide)-*block*-poly (sodium methacrylate), PEO-*block*-PMANa polyelectrolyte polymers were studied. In the absence of salt, the hydrodynamic diameters for PMOTAC and PEO-*b*-PMANa were 48 and 28 nm, respectively, whereas for PEC, at a 1:1 molar ratio, larger sizes (134 nm, and 2000-4000 nm) were obtained. In the presence of salt (20-160 mM NaCl), the hydrodynamic diameters for PMOTAC and PEO-*b*-PMANa were 44-45 and 8-10 nm, respectively, probably due to screening of surface charge by smaller counter ions. In the presence of 20, 80, and 160mM sodium chloride, 1:1 PEC complexes were relatively monodisperse with averaged hydrodynamic diameters of 93, 124, and 120 nm, respectively. With an excess of either the cationic or anionic component, non-stoichiometric complexes were formed.

The suitability of using AsFlFFF to monitor aggregation and fusion of phospholipid vesicles (liposomes) upon storage at +4 or-18 ^{o}C was studied. The vesicles were mainly egg yolk phosphatidylcholine (EPC) in the presence of 20-mol% phosphatidylserine (PS), phosphatidic acid (PA), phosphatidyl inositol (PI), and diacylphosphatidyl glycerol (PG), and 20-mol% cholesterol or 3 mM calcium chloride. After extrusion through 100nm-carbonate filter or storage at +4 ^{0}C for about five months, the average particle sizes were 122 ± 5 nm. When the storage period was extended to about eight months (250 days), larger destabilized aggregates, with a mean diameter of 215 nm, were observed. When EPC was stored at –18 ^{o}C, large particles were formed as a result of dehydration, aggregation, and fusion processes. In the presence of 3 mM calcium chloride, EPC did not form large aggregates. After the addition of 20-mol% of negatively charged phospholipids (PS, PA, PI, or PG) to the liposomes, the

electrostatic interactions with calcium ions were increased, and large aggregates were formed. Monovalent Na^{+}or Cl^{-} ions did not have such an effect. In the presence of cholesterol, large aggregates were obtained after storage at + 4 and –18 ^{o}C for more than one day.

In addition both miniaturized and conventional AsFlFFF systems were used to monitor aggregation and fusion of low-density lipoproteins (LDL). With the miniaturized AsFlFFF, it was possible to achieve retention profiles within shorter time periods, with smaller sample amounts, and with lower mobile phase consumption than with the conventional AsFlFFF. The resolutions of the peak profiles were similar in both miniaturized and conventional setups, in spite of the significant peak broadening in mAsFlFFF that resulted in lower plate heights. The miniaturized AsFlFFF was also more sensitive to mass overloading than the conventional AsFlFFF. In mAsFlFFF, changes in pH and ionic strength did not cause aggregation of LDL particles, in contrast to the treatment of LDL particles with α-chymotrypsin. In addition to vortexing, treatment with phospholipases A2, sphingomyelinase, and copper sulfate led to the formation of aggregated and/or fused LDL particles.

7. REFERENCES

1. Knoll, M., Ruska, E., *Zeitschrift fuer Physik 78* (1932) 318.
2. Heinemann, K., Poppa. H., *Appl. Phys. Lett. 16* (1970) 515.
3. Thuman-Commike, P.A., *FEBS Letter 505* (2001) 199.
4. Von Ardenne M., *Zeitschrift fuer Physik 108* (1938) 338
5. Stewart, A. D. G., *Measurement and Instrument Review 15* (200) (1968) 569.
6. Binnig, G., Rohrer, H., Gerber, Ch., Weibel, E. *Phys. Rev. Lett. 49 (*1982) 57.
7. Binnig, G., Quate, C. F., Gerber, Ch., *Phys. Rev. Lett.* 56 (1986) 930.
8. Radmacher, M., Tillamnn, R.W., Fritz, M., Gaub, H.E., *Science* 257 (1992) 1900.
9. Magonov, S. *Handbook of Surfaces and Interfaces of Materials*, 2 (2001) 393.
10. Kelley, T.W., Schorr, P.A., Johnson, K.D., Tirrell, M. Frisbie, C.D., *Macromolecules* 31 (1998) 4297.
11. Hansma, P.K., Cleveland, J.P., Radmacher, M., Walters, D. A., Hillner, P.E., Bezanilla, M., Fritz, M., Vie, D., Hansma, H.G., Prater, C.B., Massie, J., Fukunage, L., Gurley, J., Elings, V., *Appl. Phys. Lett*. 64 (1994) 1738.
12. Shao, Z., Yang, J., Somlyo, A. P. *Annu. Rev. Cell Dev. Biol.* 11 (1995) 241.
13. Martin, Y., Williams C.C, Wickramasinghe H.K., *J. Appl. Phys. 61* (1987) 4723.
14. Engel, A., Muller, D. J., *Nat. Struct. Biol.* 7 (2000) 715.
15. Dufrêne, Y. F., *Nature Methods* 3 (2006) 973.
16. Givan AL. *Flow Cytometry: First Principles, N*ew York, NY: Wiley-Liss, 1992.
17. Melamed MR. *Flow Cytometry and Sorting, N*ew York, NY: Wiley-Liss; 1990.
18. Shapiro H. *Practical Flow Cytometry*, 3rd ed. New York, NY: Alan R. Liss; 1994.
19. Mueller, P.K., Givens, R.G., *JAPCA J AIR WASTE MA 11* (1961) 576.
20. Schurr, J. M., Schmitz, K. S., *Biopolymers* 12 (1973) 1021.
21. Berne, B.J., Pecora, R., *Dynamic Light Scattering: with Applications to Chemistry, Biology, and Physics*. Wiley-Interscience, New York 1975.
22. Brown, W., *Dynamic Light Scattering: The Method and Some Applications.* Clarendon Press, Oxford 1993.
23. Finsy, R., *Adv. Ccolloid Interfac. 52* (1994) 79.
24. Plantz, P.E., *ACS Symposium Series* 693 (Particle Size Distribution III) (1998), 103.
25. Svedberg, T., Rinde, H., *J.Amer. Chem. Soc. 46* (1924) 2677.
26. Cantow, H. J., *Makromolekulare Chemie* 70 (1964) 130.
27. Laue, T. M, Stafford, W. F., *Annu. Rev. Bioph. Biom.* 28 (1999) 75.
28. Brown, P.H, Schuck, P., *Biophys. J. 90* (2006) 4651.
29. Lebowitz J., Lewis M.S., Schuck P., *Protein Sci, 11* (2002) 2067.
30. Small, H., Langhorst, M.A., *Anal. Chem.* 54 (1982) 892A-894A, 896A-898A.
31. McGowan, G.R., Langhorst, A.L., *J. Coll. Interface Sci. 89* (1982) 94.

32. McHugh, A.J., Hydrodynamic chromatography. In: Hunt, B.J., Holding S.R., Editors, *Size Exclusion Chromatography*, Chapman and Hall, New York 1989, pp. 248–270.

33. Venema, E., Kraak, J. C., Poppe, H., Tijssen, R., *J. Chromatogr. A* 740 (1996) 159.

34. Smith, I., *Chromatographic and Electrophoretic Techniques,* vol. 2, Heineman Medical Books, London 1976.

35. O'Farrell, P.H., *J. Biol. Chem.* 250 (1975) 4007.

36. Zhou, F., Johnston, M. V., *Anal. Chem. 76 (*2004) 2734.

37. Klose, J., Kobalz, U., *Electrophoresis 16 (*1995) 1034.

38. Righetti, P.G., Castagna, A., Herbert, B., *Anal. Chem. 73* (2001) 320A.

39. Issaq, H.J., *Electrophoresis* 22 (2001) 3629.

40. Hsieh, M.-M., Tseng, W.-L., Chang, H.-T., Electrophoresis 21 (2000) 2904.

41. Jin, Y., Lin, B., Fung, Y. S., Electrophoresis 22 (2001) 2150.

42. Lin, Y.-W., Chang, H.-T., ., *J. Chromatogr. A* 1130 (2006) 206.

43. Litzén, A., Wahlund, K.G., *J. Chromatogr. 476* (1989) 413.

44. Wahlund, K.G., Litzén A., *J. Chromatogr*. 461 (1989) 73.

45. Li, P., Hansen, M., Giddings, J.C., *J. Liq. Chromatogr. R.T.* 20 (1997) 2777.

46. Nilsson, M., Bulow, L., Wahlund K.-G. *Biotechnol Bioeng. 54* (1997) 461.

47. Moon, M.H., Park, I., Kim, Y., *J. Chromatogr. A 813* (1998) 91.

48. Lee, H., Williams, S. K.R., Allison, S.D., Anchordoquy, T.J., *Anal. Chem.* 73 (2001) 837.

49. Giddings, J.C., *Sep. Sci.* 1 (1966) 123.

50. Berg, H.C., Bruce, E.M., *Proc Natl Acad Sci USA 5*8 (1967) 1286.

51. Giddings, J. C., *Science* 260 (1993) 1456.

52. Giddings, J.C., Yang, F.J., Myers, M.N. *Anal. Chem.* 46 (1974) 1917.

53. Giddings, J.C., Myers, M.N., Caldwell, K D., Fisher, S.R., *Method Biochem Anal.* 26 (1980) 79.

54. Koliadima, A., Karaiskakis, G. *J. Liq. Chromatogr. 11* (1988) 2863.

55. Bailin, C., Charles, A.S., Beckett, R., *J. Environ. Monit. 3* (2001) 7.

56. Kirkland, J.J., Rementer, S.W., Yau, W.W. *Anal. Chem. 53,* (1981) 1730.

57. Kirkland, J.J., Yau, W.W., Doerner, A., Grant, J. W. *Anal. Chem. 52* (1980) 1944.

58. Kirkland, J.J., Yau, W.W., Doerner, W.A., Grant, J.W. *J. Chromatogr. 255* (1983) 255.

59. Openheimer, L.E., Mourey, T.H. *J. Chromatogr. 298* (1984) 217.

60. Giddings, J.C., Moon, M.H., Williams, P.S., Barman, B.N. (1991): Particle separation and size characterisation by sedimentation field-flow fractionation. In: Provder T. (ed) particle size distribution, American Chemical society, Washington DC, pp 199-216.

61. Hassellöv, M., Lyvén, B., Bengtsson, H., Jansen, R., Turner, D.R., Beckett, R. *Aquat. Geochem. 7(2)* (2001) 155.

62. Blo, C., Contado, F., Fagioli, M.H., Rodriguez, B., Dondi, F. *Chromatographia 41*(1995) 715.

63. Yang, F.S., Caldwell, K.D., Giddings, J.C. *J. Colloid interface Sci. 92* (1983) 81.

64. Giddings, J.C., Yang F.S. *J. Colloid Interface Sci., 105* (1985) 55.

65. Janca, J., Pribylova D., Bouchal K., Trackova V., Zurkova E. *J. Liq. Chromatogr. 9* (1986) 2059.

66. Ran, Y., Fu J.M., Sheng, G.Y., Beckett, R., Hart B.T. *Chemosphere 41* (2000) 33.

67. Yong, R., Jia-Mo F., Guo-ying, S., Beckett, R., Hart, B.T., *Environ. Sci. 12* (2000) 129.

68. Metreau, J. M., Gallet, S., Cardot, P.J.P., LeMarie, V., Dumas, F., Hernvann, A., Loric, S. *Anal. Biochem. 251 (1997) 178.*

69. Sanz, R., Puignou, L., Reschiglian, P., Galceran, M.T. *J. Chromatogr. A 919* (2001) 339.

70. Beckett, R., Ho, J., Jiang, Y., Giddings, J.C., *Langmuir 7* (1991) 2040.

71. Jones, K. K., Barman, B.H., Giddings, J. C. *J. Chromatogr.* 455 (1988) 1.

72. Andersson, M., Fromell, K., Gullberg, E., Artursson, P., Caldwell, K.D., *Anal. Chem.* 77 (2005) 5488.

73. Thompson, G.H., Myers, M.N., Giddings, J.C., *Sep. Sci. 2* (1967) 797.

74. Thompson, G.H., Myers, M.N., Giddings, J.C., *Anal. Chem. 41* (1969) 1219.

75. Giddings, J.C., Caldwell, K.D., Myers, M.N., *Macromolecules 9* (1976) 106.

76. Williams, P.S., Giddings, J.C., *Anal. Chem. 59* (1987) 2038.

77. Lee, S., *J. Microcolumn. Sep. 9* (1997) 281.

78. Pasti, L., Bedani, F., Contado, C., Mingozzi, I., Dondi, F., *Anal. Chem.* 76 (2004) 6665.

79. Williams, S. K.R., Lee, D., *J. Sep. Sci.* 29 (2006) 1720.

80. Kasparkova, V., Halabalova, V., Simek, L., Dostal, J., Janca, J., *J. Liq. Chromatogr. R.T.* 29 (2006) 2771.

81. Caldwell, K.D., Kesner, L.F., Myers, M.N., Giddings, J.C., *Science 176,* (1972) 296.

82. Caldwell, K.D., Gao, Y.S., *Anal. Chem. 65 (*1993) 1764.

83. Tri, N., Caldwell, K., Beckett, R., *Anal. Chem. 72 (*2000) 1823.

84. Edwards, T., Gale, B.K., Frazier, A.B., *Biomed. Microdevices* 3 (2001) 211.

85. Gale, B.K., Caldwell, K.D., Frazier, B.A., *Anal. Chem.* 74 (2002), 1024.

86. Lao, A.I.K., Lee, Y.-K., Hsing, I-M., *Anal. Chem.* 76 (2004) 2719.

87. Giddings, J.C., Yang, F.J., Myers, M.N., *Anal. Chem.* 48 (1976) 1126.

88. Giddings, JC, Yang, F.J., Myers, M.N., *Science* 193 (1976) 1244.

89. Ratanathanawongs-W., S.K. In *Field-Flow Fractionation Handbook*; Schimpf, M.E., Caldwell, K.D., Giddings, J.C., Eds.; Wiley-Interscience: New York, 2000; Chapter 17.

90. Liu, M.-K., Li, P., Giddings, J.C., *Protein Sci.* 2 (1993) 1520.

91. Giddings J.C., *J. Chem. Edu.*50 (1973) 667.

92. Giddings, J.C., Chen, X., Wahlund, K.-G., Myers, M.N., *Anal. Chem* 59 (1987) 1957.

93. Ratanathawongs, S. K., Giddings, J.C., *Anal. Chem.* 64 (1992) 6.

94. Granger, J., Dodds, J., Leclerc, D., Midoux, N., *Chem. Eng. Sci. 41* (1986) 3119.

95. Wahlund, K.G., Giddings, J.C., *Anal. Chem.* 59 (1987) 1332.

96. Litzén, A., Wahlund, K.-G., *J. Chromatogr.* 548 (1991) 393.

97. Litzén, A., Wahlund, K.-G., *Anal. Chem.* 63 (1991) 1001.

98. Litzén, A., Walter, J.K., Krischollek, H., Wahlund, K.-G., *Anal. Biochem.,* 212 (1993) 469.

99. Yohannes, G., Wiedmer, S.K., Tuominen, E. K. J., Kinnunen, P. K. J., Riekkola, M.-L. *Anal. Bio. Chem*. 380 (2004) 757.

100. Giddings, J.C., Lin, G.-C., Myers, M.N. *J. Liq. Chromatogr*. 1 (1978) 1.

101. Benincasa, M. A., Giddings J. C. *Anal. Chem. 64* (1992) 790.

102. Kirkland, J.J., Dilks, C.H.Jr., Rementer, S.W., *Anal. Chem. 64* (1992) 1295.

103. Wittgren, B., Wahlund, K.-G., Derand, H., Wesslen, B. *Macromolecules, 29* (1996) 268.

104. Wittgren, B., Wahlund, K.-G., Derand, H., Wesslen, B. *Langmuir 12* (1996) 5999.

105. Hecker, R., Fawell, P.D., Jefferson, A., Farrow, J. B., *J. Chromatogr. A 837* (1999) 139.

106. Benincasa, M. A., Caldwell, K. D., *J. Chromatogr. A 925* (2001) 159.

107. Giddings, J.C., Yang, F.J., Myers, M.N., *Anal. Biochem.* 81 (1977) 395.

108. Song, J.H., Kim, W.-S., Park, Y.H., Yu, E.K., Lee, D.W., *Bull. Korean Chem. Soc., 20* (1999) 1159.

109. Udabage, P., Sharma, R., Murphy, D., McKinnon I., Beckett, R., *J. Microcol. Sep* (1997) 557.

110. Jussila, M.A., Yohannes, G., Riekkola, M.-L. *J. Microcol. Sep 9* (1997) 601.

111. Wahlund, K.-G., Gustavsson, M, MacRitchie, F., Nylander, T., Wannerberger L., *J. Cereal Sci. 23* (1996) 113.

112. Stevenson, S.G., Ueno, T., Preston, K.R., *Anal. Chem. 71*, (1999) 8.

113. Liu, M.-K., Giddings, J.C., *Macromolecules 26* (1993) 3576.

114. Moon, M. H., Giddings, J.C., *J. Pharm. Biomed. Anal. 11* (1993) 911.

115. Korgel, B.A., Van Zanten, J.H., Monbouquette, H.G. *Biophys. J. 74* (1998) 3264.

116. Nilsson, M., Wahlund, K.-G, Birnbaum, S., *J. Biochem. Biophys. Meth. 33* (1996) 9.

117. Nilsson, M., Wahlund, K.-G., Bilow, L. *Biotechnol. Tech. 12* (1998) 477.

118. Frankema, W., van Bruijnsvoort, M., Tijssen R., Kok W. T. *J. Chromatogr. A 943* (2002) 251.

119. Tank, C., Antonietti, M., *Macromol. Chem. Phys., 197* (1996) 2943.

120. Moon, M.H.; Kwon, H., Park, I. *Anal. Chem 69* (1997) 1436.

121. Ratanathawongs, S.K.; Giddings J.C. *Polym. Mater. Sci. Eng. 70* (1993) 26.

122. Beckett, R., Jue, Z., Giddings, J.C. *Environ. Sci. Technol. 21* (1987) 289.

123. Dycus, P.J.M., Heal, K.D., Stearman, G.K., Wells, M. J.M. *Sep. Sci. Technol. 30* (1995) 1435.

124. Schimpf, M. E., Wahlund, K.-G. *J. Microcolumn. Sep 9* (1997) 535.

125. Kammer, F.V.D., Förstner, U. *Wat. Sci. Tech. 37* (1998) 173.

126. Vaillancourt, R.D., Balch, W.M. *Limnol. Oceanogr.45* (2000) 485.

127. Exner, A, Theisen M., Panne, U., Niessner, R. *Fresenius J. Anal. Chem., 366* (2000) 254.

128. Dahlqvist, R, Benedetti, MF, Andersson, K., Turner, D., Larsson, T., Stolpe, B., Ingri. J. *Geochimica et Cosmochimica* 68 (2004) 4059.

129. Yohannes, G., Wiedmer, S. K., Jussila, M., Riekkola, M.-L. *Chromatographia* 61 (2005) 359.

130. Baalousha, M.,von der Kammer, F., Motelica-Heino, M., Le Coustumer, P., *J. Chromatogr. A* 1093 (2005) 156-166.

131. Baalousha, M., Lead, J.R., *Environ. Sci. Technol.* 41 (2007) 1111.

132. Luo, J., Leeman, M., Ballagi, A., Elfwing, A., Su, Z., Janson, J.-C., Wahlund, K-G., *J. Chromatogr. A* 1120 (2006) 158.

133. Jönsson, J. -Å., Carlshaf, A. *Anal. Chem.* 61 (1989) 11.

134. Park, I., Paeng, K.-J., Kang, D., Moon M.H. *J. Sep. Sci.* 28 (2005) 2043.

135. Giddings, J.C., Williams, P. S., Benincasa, M.A. *J. chromatogr*. 627 (1992) 23.

136. Caldwell, K.D, Field-flow fractionation of particles. In Modern Methods of Particle Size Analysis, Howard G. Barth, Ed., Chemical Analysis, Vol. 73: A Wiley-Interscience publication, John Wiley and Sons, New York, 1984, Chapter 7.

137. Schure, M.R., Barman, B.N., Giddings, J.C. *Anal. Chem* 61 (1989) 2735.132.

138. Joe, M.D., Band broadening and plate height. In *Field-Flow Fractionation Handbook*; Schimpf, M.E., Caldwell, K.D., Giddings, J.C., Eds.; Wiley-Interscience: New York, 2000; Chapter 3.

139. Giddings, J.C., Yoon, Y.H., Caldwell, K.D., Myers, M.N., Hovingh, M.E., *Sep. Sci.* 10 (1975) 447.

140. Giddings, J.C., *Unified Separation Science*, Wiley, New York 1991, pp. 210.

141. Giddings, J.C., Schure, M.R., Myers, M.N., Velez, G.R., *Anal. Chem.* 56 (1984) 2099.

142. Giddings, J.C., Schure, M.R, *Chem. Eng. Sci.* 42 (1987) 1471.

143. Williams, P.S., Giddings, S.B., Giddings, J.C., *Anal. Chem.* 58 (1986) 2397.

144. Giddings, J.C. *Anal. Chem.* 62 (1990) 2306.

145. Said, A.S., *Theory and mathematics of chromatography*. Heidelberg, Germany: Dr. Alfred Huethig Publishers, 1981.

146. Yau, W.W., Kirkland, J.J., Bly, D.D. *Modern Size-Exclusion Liquid Chromatography*; Wiley-Interscience: New York, U. S. A., 1979.

147. MacDonald, R.C., MacDonald, R.I., Menco, B.P., Takeshita, K., Subbarao, N.K., Hu, L.R., *Biochim Biophys Acta* 1061 (1991) 297.

148. Kucerka, N., Kiselev, M.A., Balgavy, P., *Eur. Biophys. J. 33* (2004) 328.

149. Saccani, J., Castano, S., Desbat, B., Blaudez, D., *Biophys. J.* 85 (2003) 3781.

150. Pascher, T., Chesick, J.P., Winkler, J.R., Gray, H.B. *Science 271* (1996) 1558.

151. Naeem, A., Khan, R.H., *Int. J. Biochem. Cell B. 36* (2004) 2281.

152. Wijnhoven, J.E.G.J., Koorn, J.-P., Poppe, H., Kok, W.T. *J Chromatogr. A.* 732 (1996) 307.

153. H.C. Bundenberg de Jong, *Colloid Sci.*, Elsevier, Amsterdam 1949.

154. Michaels, A.S., Mir, L., Schneider, N.S., *J. Phys. Chem.* 69 (1965) 1447.

155. Veis, A., Biological Polyelectrolytes, New York 1970.

156. Buchhammer, H.-M., Kramer, G., Lunkwitz, K., *Colloid Surf A 95* (1994) 299.

157. Pinteala, M., Budtova, T., Epure, V., Belnikevich, N., Harabagiu, V., Simionescu, B.C. *Polymer* 46 (2005) 7047.

158. Tsuchida, E. *J Macromol. Sci. Pure Appl. Chem.* A31 (1994) 1.

159. Saeki, S., Kuwahara, N., Nakata, M., Kancko, M. *Polymer* 17 (1976) 685.

160. Child, H. G. *Prog. Polym. Sci. 17 (*1992) 163.

161. Klug, E. D. J. *Polym. Sci. Part G 36 (*1971) 491.

162. Eisele, M., Burchard, W. *Makromol. Chem.191 (*1990) 169.

163. Badiger, M. V.; Lutz, A.; Wolf, B. A. *Polymer 41(* 2000) 1377.

164. Eeckman, F., Moës, A.J., Amighi, K., *Int. J. Pharmaceutics* 241 (2002) 113.

165. Zhang, X.-Z., Zhuo, R.-X., Cui, J.-Z., Zhang, J.-T. Int. J. Pharmaceutics 235 (2002) 43.

166. Kikuchi, A., Okano, T., in: Bio related Polymers and Gels: Controlled Release and Applications in Biomedical Engineering (Polymers, Interfaces and Biomaterials), T. Okano (Ed.), Academic Press, San Diego, 1998, pp. 1-28.

167. Kawaguchi, H., Kisara, K., Takahashi, T., Achiha, K., Yasui, M., *Macromol. Symp.* 151 (2000) 591.

168. Su, P., Wang, Y.-C., Zhang, X.-X., Sun. L., Chang, W.-B., *Anal. Chim. Acta* 418 (2000) 137.

169. Wiedmer, S.K., Riekkola, M.-L., Tenhu, H. *J. Cap. Elec. Microchip Technol.* 6 (1999) 163.

170. Qiu, X., Kwan, C.M.S., Wu, C. *Macromolecules* 30 (1997) 6090.

171. Wu, C., Zhou, S. *Macromolecules* 30 (1997) 574.

172. Wang, X., Qiu, X., Wu, C., *Macromolecules* 31 (1998) 2972.

173. Virtanen, J., Holappa, S., Lemmetyinen, H., Tenhu, H. *Macromolecules* 35 (2002) 4763.

174. Siu, M.-H., Zhang, G., Wu, C. *Macromolecules* 35 (2002) 2723.

175. Otake, K., Karaki, R., Ebina, T., Yokoyama, C., Takahashi S., *Macromolecules 26 (*1993) 2194.

176. Virtanen, J., Tenhu, H. *Macromolecules* 33 (2000) 5970.

177. Bangham, A.D., Horne, R.W. *J Mol Biol.* 8 (1964) 660.

178. Torchilin, V.P. *Nat. Rev. Drug Discov.* 4 (2005) 145.

179. Ulrich, A.S. *Bioscience Rep.* 22 (2002) 129.

180. Chrai, S.S., Murari, R., Ahmad, I. *Pharmaceutical Technology Europe* 15 (2003) 53.

181. Casals, E., Galan, A.M., Escolar, G., Gallardo, M., Estelrich, J. *Chem. Phys. Lipids*, 125 (2003) 139.

182. Winterhalter, M., Lasic, D.D. *Chem. Phys. Lipids* 64 (1993) 35.

183. Segota, S., Tezak, D., Ljubesic, N. *Adv. Colloid. Interfac. 89-90* (2001) 283.

184. Heimburg, T., Marsh, D. *Biophys J.* 68 (1995) 536.

185. Rytömaa, M., Mustonen, P., Kinnunen, P.K.J. *J. Biol. Chem. 267* (1992) 22243.

186. Kawai, C., Prado, F.M., Nunes, G.L.C., Di Mascio, P., Carmona-Ribeiro, A.M., Nantes, I.L. *J Biol Chem.* 280 (2005) 34709.

187. Kinnunen, P.K.J., Köiv, A., Lehtonen, J.Y.A., Rytömaa, M., Mustonen, P. *Chem. Phys. Lipids* 73 (1994) 181.

188. Rytömaa, M., Kinnunen, P.K.J. *J. Biol. Chem.* 269 (1994) 1770.

189. Rytömaa, M., Kinnunen, P.K.J. *J Biol. Chem.* 270 (1995) 3197.

190. Tuominen, E.K.J., Wallace, C.J.A., Kinnunen, P.K.J. *J Biol Chem*. 277 (2002) 8822.

191. Bychkova, V.E., Pain, R.H., Ptitsyn, O.B. *FEBS Lett* 238 (1988) 231.

192. Ptitsyn, O.B., Pain. R.H., Semisotnov, G.V., Zerovnik, E., Razgulyaev, O.I. *FEBS Lett* 262 (1990) 20.

193. Ohgushi, M., Walda, A. *FEBS Lett* 164 (1983) 21.

194. Hamada, D., Kuroda, Y., Kataoka, M., Aimoto, S., Yoshimura, T., Goto, Y. *J Mol Biol* 256 (1996) 172.

195. Yoshimoto, M., Walde, P., Umakoshi, H., Kuboi, R. *Biotechnol Prog* 15 (1999) 689.

196. Thuenemann, A. F., Mueller, M., Dautzenberg, H,. Joanny, J.-F., Loewen, H., *Adv. Polym. Sci.* 166 (2004) 113.

197. Kabanov, V.A., Zezin, A.B. *Pure Appl Chem* 56 (1984) 343.

198. Kovacevic, D., Borkovic, S., Pozar, J. *Colloid Surface A* 302 (2007) 107.

199. Pergushov, D.V., Buchhamer, H.-M., Lunkwitz, K. *Colloid Polym. Sci.* 277 (1999) 101.

200. Holappa, S., Andersson, T., Kantonen, L., Plattner, P., Tenhu H. *Polymer* 44 (2003) 7907.

201. Schultz, R.M., Liebman, R.B., *Proteins: Composition and structure*, In Devlin TM (ed), *Textbook of biochemistry with clinical correlation*, 5 ed. Wiley, Lissabon 2002, pp 127-130.

202. Williams, K.J., Tabas, I., *Arterioscler. Thromb. Vasc. Biol.* 15 (1995) 551.

203. Williams, K.J., Tabas, I. *Curr. Opin. Lipidol.* 9 (1998) 471.

204. Öörni, K., Pentikäinen, M.O., Ala-Korpela, M., Kovanen P.T. *J. Lipid Res.* 41 (2000) 1703.

205. Schissel, S.L., Tweedie-Hardman, J., Rapp, J.H., Graham, G., Williams, K.J., Tabas I., *J. Clin. Invest.* 98 (1996) 1455.

206. Paananen, K. Kovanen, P.T., *J. Biol. Chem.* 269 (1994) 2023.

207. Pentikäinen, M.O., Lehtonen, E.M., Kovanen P.T. *J. Lipid Res.* 37 (1996) 2638.

208. Öörni, K., Posio, P., Ala-Korpela M., Jauhiainen, M. and Kovanen P.T. *Arterioscl. Thromb. Vasc Biol.* 25 (2005) 1678.

209. Goñi, F.M., Alonso, A. *FEBS Lett.* 531 (2002) 38.

210. Marathe, S., Schissel, S.L., Yellin, M.J., Beatini N., Mintzer R., Williams K.J., Tabas, I., *J. Biol. Chem.* 273 (1998) 4081.

211. Khoo J.C., Miller, E., McLoughlin, P., Steinberg, D, *Arteriosclerosis* 8 (1988) 348.

212. Guyton, J.R., Klemp, K.F., Mims, M.P., *J. Lipid Res.* 32 (1991) 953.

213. Tanford C., *Physical Chemistry of Macromolecules*, Wiley, New York 1961, de Gennes, P.-G. *Scaling concept in polymer physics*, Cornell University Press; Ithaca, NY, 1979.

214. Laguna, M.T.R., Medrano, R., Plana, M.P., Tarazona, M. P., *J. Chromatogr. A.* 919 (2001) 13.

215. Litzén, A (1992) *Asymmetrical Flow Field-flow fractionation*, Doctoral dissertation, Comprehensive Summaries of Uppsala dissertations from the Faculty of Pharmacy 93. Univ. of Uppsala.

216. Gabrielson, J. P., Brader, M. L., Pekar, A. H., Mathis, K. B., Winter, G., Carpenter, J. F., Randolph, Th. W. *J. Pharm Sci.* 96 (2006) 268.

217. Duval, C., Le Cerf, D., Picton, L., Muller, G., *J. Chromatogr. B.* 753 (2001) 115.